Precambrian Research 325 (2019) 1–19

Contents lists available at ScienceDirect

Precambrian Research

journal homepage: www.elsevier.com/locate/precamres

Provenance and tectonic implications of the 3.28–3.23 Ga Fig Tree Group, central Barberton greenstone belt, South Africa

Nadja Drabon[a,*], Aleksandra Galić[b,1], Paul R.D. Mason[b], Donald R. Lowe[a]

[a] Department of Geological Sciences, Stanford University, 450 Serra Mall, Stanford, CA 94305, USA
[b] Utrecht University, Department of Earth Science, Princetonlaan 8A, 3584 CB Utrecht, the Netherlands

A B S T R A C T

Sedimentary rocks provide a valuable record of non-uniformitarian Paleoarchean tectonic processes. The rocks of the 3.28–3.23 Ga Mapepe Formation mark the initiation of orogenesis in the Barberton Greenstone Belt, South Africa. However, reconstruction of the Mapepe basin(s) is challenging because the rocks occur in fault-bounded structural belts that are characterized by lateral heterogeneity and whose correlation remains uncertain. We have studied the petrography, geochemistry, and detrital zircon geochronology from outcrop and drill core samples from two adjacent structural belts, the Manzimnyama Syncline and the Eastern Barite Valley area, to evaluate the timing of basin formation, correlate between these two adjacent areas, and provide constraints on the character of tectonic uplift.

In the Eastern Barite Valley area sedimentation was initiated at about 3260 Ma. The section includes a lower, deep-water unit of mainly mudstone overlain by a shoaling-upward sequence of fan-delta sandstone and conglomerate. The sandstone throughout the formation was derived by erosion of local uplifts of the underlying greenstone-belt sequence except at the top of the section where sedimentation was dominated by dacitic volcaniclastic sediments dated at 3239 Ma. In contrast, rocks of the Mapepe Formation in the Manzimnyama Syncline area, 1–2 km south of the Eastern Barite Valley area, record the initiation of sedimentation at about 3277 Ma with deposition of a rhyolitic tuffaceous unit followed by persistent deep-water sedimentation of banded iron formation, banded ferruginous chert, and turbiditic sandstone. Siliciclastic sediments are immature and were derived by erosion of older supracrustal greenstone-belt rocks. No Fig Tree age volcanism younger than 3260 Ma is recorded in this belt.

Overall, Mapepe sedimentary rocks record the formation of numerous local uplifts of underlying supracrustal rocks with periodic volcanic activity, and the dispersal of debris to form mainly small fan-deltas flanked by deep-water systems. The contrasting ages, lithologies, depositional settings, and provenance of the sedimentary rocks in the now adjacent Eastern Barite Valley and Manzimnyama Syncline belts suggest that they were deposited in either different parts of a large, complex Fig Tree basin or represent separate basins that have been juxtaposed during post-Fig Tree tectonism and shortening.

1. Introduction

The 3.2 Ga Mapepe Formation of the Fig Tree Group in the Barberton Greenstone Belt (BGB), southern Africa, is part of the Barberton Supergroup (Fig. 1), one of the oldest well-preserved volcanic and sedimentary sequences on Earth. It marks the first appearance of orogenic siliciclastic sediments in the BGB, derived from uplift, deformation, and erosion of the underlying Onverwacht Group that records 300 million years of basaltic and komatiitic volcanism and general tectonic quiescence (Lowe, 1999). Paleogeographic and tectonic reconstructions of the sedimentary basin or basins in which the sediments and volcaniclastics of the Mapepe Formation accumulated, however, are difficult due to syn- and post-depositional tectonics and the resulting present fragmented character of exposed strata. The Mapepe Formation is exposed in numerous, mainly synclinal structural belts that make up part of the central BGB and are separated by faulted anticlinal belts of the Onverwacht Group and shear zones of unknown displacement (Figs. 1 and 2). The stratigraphic sections within these belts commonly differ significantly in depositional settings (Lowe et al., 1999) and the reconstruction of early basin geometries and configurations remains challenging.

This study focuses on samples taken from the International Continental Scientific Drilling Program (ICDP) drill cores BARB4 from the extensively studied and well-preserved Manzimnyama Syncline (MS) and BARB5 from the Eastern Barite Valley (EBV), two closely juxtaposed structural belts in the eastern part of the BGB (Figs. 1 and 2). Both cores penetrate Mapepe strata. Here we assess the stratigraphy and provenance of sedimentary rocks of the Mapepe Formation in these belts. A comparative provenance analysis of these two adjacent structural belts allows the correlation between these two contrasting sections of the Mapepe Formation to be tested, coupled with dating of the onset of basin formation, evaluating the nature of the tectonic uplifts that sourced the sediments, and constraining the spatial and temporal relationships of these belts. The results will contribute to the

* Corresponding author.
E-mail address: drabon@stanford.edu (N. Drabon).
[1] Present address: Utrecht University, Copernicus Institute of Sustainable Development, Princetonlaan 8A, 3584 CB Utrecht, the Netherlands.

https://doi.org/10.1016/j.precamres.2019.02.010
Received 26 July 2018; Received in revised form 4 February 2019; Accepted 12 February 2019
Available online 13 February 2019
0301-9268/

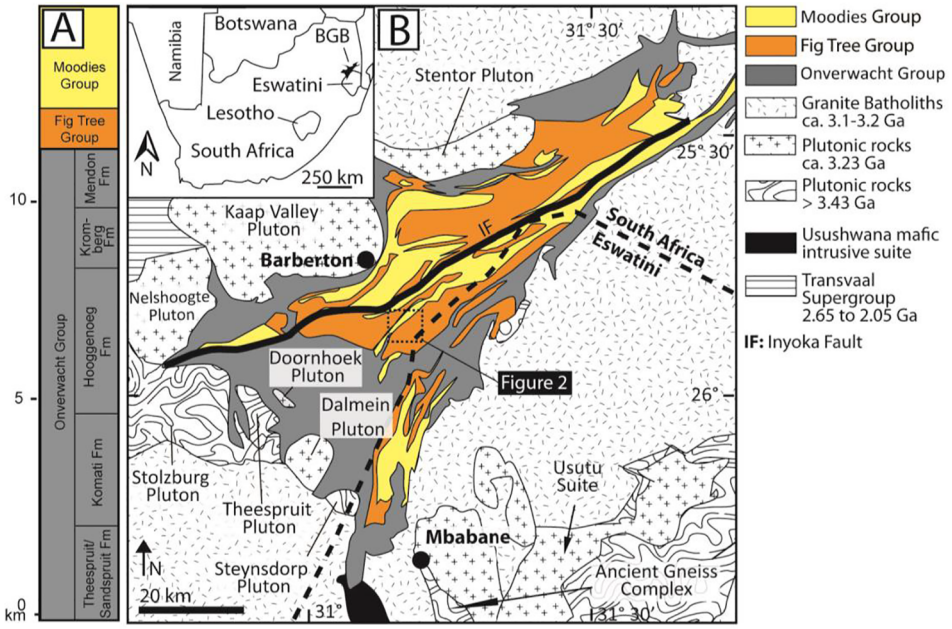

Fig. 1. [A] Stratigraphic column of the Barberton Supergroup. [B] Simplified geologic map of the Barberton Greenstone Belt and vicinity (after Anhaeusser et al., 1983).

understanding of the character of tectonic processes during the Paleoarchean.

2. Geologic setting and previous studies

2.1. Stratigraphy of the BGB and vicinity

Supracrustal rocks forming the Barberton Supergroup are located near the eastern margin of the Kaapvaal Craton in north-eastern South Africa and eSwatini, formerly known as Swaziland (Fig. 1). The 3.55–3.22 Ga BGB is composed of three stratigraphic units: from base to top, the Onverwacht, Fig Tree, and Moodies Groups. The 3552–3260 Ma Onverwacht Group represents almost 300 million years of basaltic and komatiitic volcanism punctuated by at least two phases of dacitic to rhyolitic volcanism and emplacement of co-magmatic tonalite-trondhjemite-granodiorite (TTG) plutons and shallow hypabyssal plutonic units. These felsic igneous stages are represented by dacitic to rhyolitic volcanic units in the ~3.53 Ga Theespruit Formation and the ~3.45 Ga member H6 of the Hooggenoeg Formation (Fig. 1A; see Lowe, 1999, and references within). Other episodes of felsic igneous activity, perhaps more distant, are suggested by the presence of thin dacitic tuffs and detrital zircon grains. These include felsic tuff units of 3.34 Ga in the Kromberg Formation (Byerly et al., 1996) and of 3.30–3.28 Ga in the Mendon Formation (Decker et al., 2015), as well as the presence of a major 3.30–3.28 Ga detrital zircon U-Pb age cluster in the Fig Tree and Moodies Groups (Drabon et al., 2017). The overlying Fig Tree and Moodies Groups record an abrupt change to an orogenic tectonic setting dominated by uplift of the greenstone belt sequence and, subsequently, during Moodies deposition, of deeper-seated intrusive rocks, mainly TTGs, and accompanying deposition of siliciclastic and subordinate felsic volcaniclastic sediments (Heubeck and Lowe, 1994; Lowe and Nocita, 1999; Hessler and Lowe, 2006).

In most areas, sedimentary structures are exceptionally well preserved although rocks of the BGB have experienced alteration, low-grade metamorphism, and severe deformation. Local to regional recrystallization and metasomatic alteration caused removal of Ca, Mg, Fe, and Na and addition of Si, K, and Rb, and local carbonatization (e.g., Duchac and Hanor, 1987; Toulkeridis et al., 1998; Hofmann, 2005). The rocks have been widely heated to about 300–325 °C, representing lower greenschist grade metamorphism (De Ronde et al., 1991; Xie et al. 1997; Toulkeridis et al., 1998; Tice et al., 2004). Due to severe deformation the rocks in the central BGB are now exposed as a NE-SW striking fold-and-thrust belt (Heubeck and Lowe, 1994; De Ronde and Wit, 1994; Kisters et al., 2003). The bulk of the central BGB is made up of Moodies and Fig Tree strata forming tight, commonly overturned synclines separated by narrow, sheared and faulted anticlines of serpentinized komatiitic rocks of the Onverwacht Group.

Lowe et al. (1999) divided the BGB into several fault-bounded domains, each with a distinctive stratigraphy and tectonic history: The Northern (ND), West-Central (WCD), East-Central (ECD), and Southern Domains (SD). East and southeast of the BGB (Fig. 1), the 3.66–3.20 Ga Ancient Gneiss Complex (AGC) of eSwatini contains deformed granitoid gneisses, TTGs, and interlayered amphibolites (Hunter et al.,1978; Jackson et al., 1987). It is separated from the BGB by the 3.1 Ga Mpuluzi granite but a small enclave of AGC-type rocks, the Phophonyane Inlier, is in faulted and sheared contact with the BGB. Several authors have proposed that the AGC served as a basement for the BGB (Kröner et al., 2016) or was juxtaposed against the BGB during accretion as early as 3.43 Ga (Grosch et al., 2011) or as late as 3.23 Ga (e.g., Schoene et al., 2008; Van Schijndel et al., 2017). Parts of the AGC may thus have served as a source of siliciclastic sediments to the Mapepe basin(s).

2.2. Fig Tree Group

Rocks of the Fig Tree Group are subdivided based on their location north or south of the Inyoka Fault (Fig. 1). The Ulundi, Sheba, Belvue Road, Bien Venue, and Schoongezicht Formations north of the Inyoka Fault contrast stratigraphically and lithologically with rocks of the Mapepe and Auber Villiers Formation south of this fault (Lowe, 1999). A correlation between the northern and southern Fig Tree facies remains uncertain.

North of the Inyoka Fault, rocks of the 20–50-m-thick Ulundi Formation consist of black carbonaceous mudstone, banded cherty units, banded ferruginous chert, and sparse jaspilite (Reimer, 1983). The overlying 500–1000 m-thick Sheba Formation is composed of immature lithic sandstone with subordinate siltstone and mudstone deposited largely by turbidity currents (Reimer, 1967, 1975; Condie et al.,

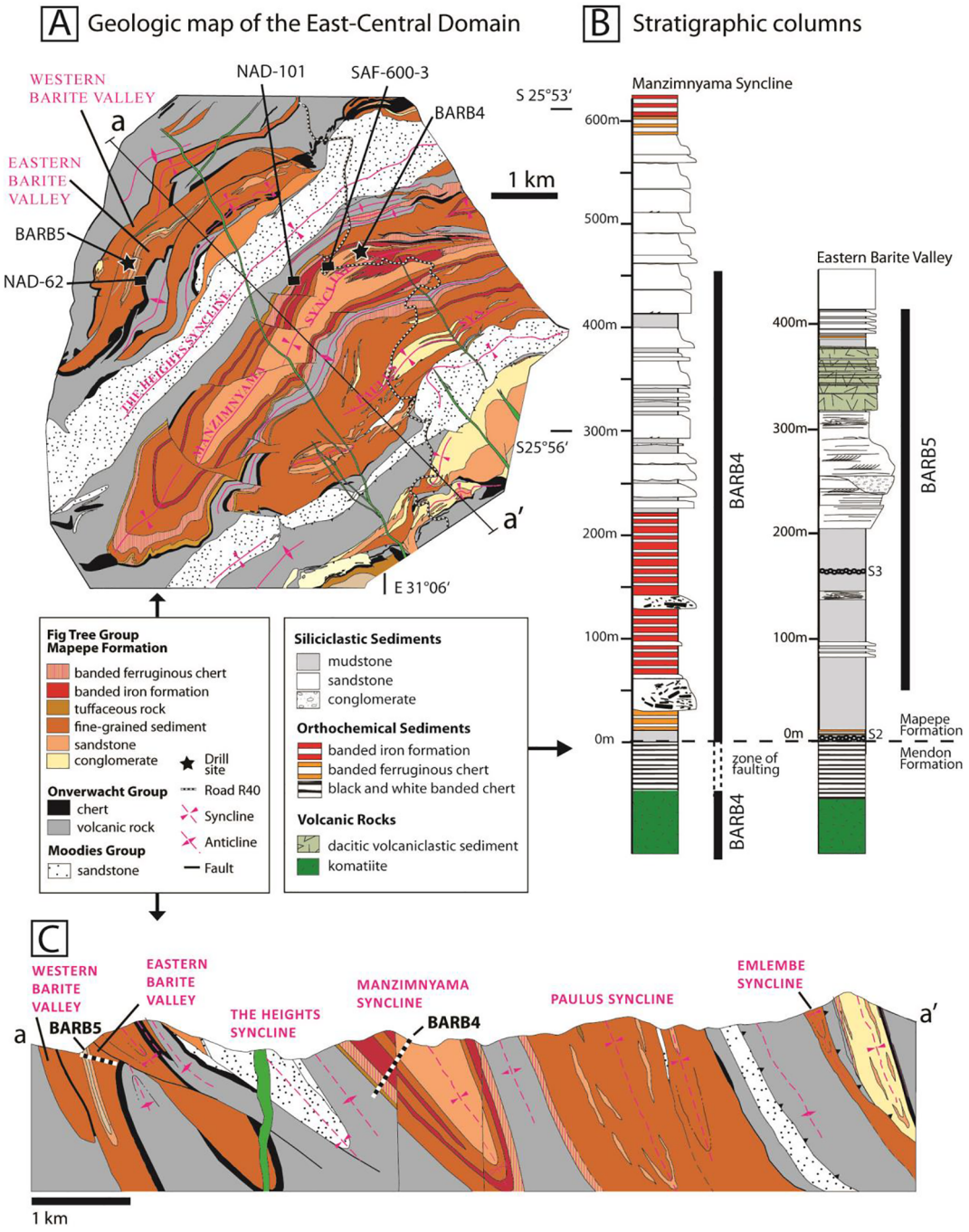

Fig. 2. [A] Geologic map of the East-Central Domain of the Barberton greenstone belt after Lowe et al. (2012). [B] Stratigraphy of the Mapepe Formation in the MS (Zentner, 2014) and the EBV (this study). [C] Cross-section of the East-Central Domain modified from Lowe et al. (2012). Drill cores are projected into the cross-section.

1970). Both units were deposited under deep-water conditions that persisted during subsequent deposition of the felsic volcaniclastic sediment, sandstone, and mudstone of the ca. 600 m thick Belvue Road Formation (Condie et al., 1970). In the western BGB, rocks of the Schoongezicht Formation are separated from those of the Sheba and Belvue Road Formations by a regional thrust fault and may be partial time-equivalents (Lowe, 1999). They form a 450 m thick sequence composed mainly of plagioclase-rich volcaniclastic conglomerate, sandstone, and gray mudstone (Condie et al., 1970; Lowe, 1999) that is overlain by basal conglomerate of the Moodies Group. Another Fig Tree unit, the Bien Venue Formation, known only from one area about 50 km northeast of Barberton, includes felsic and intermediate volcanic and volcaniclastic rocks that have yielded zircons ages of 3256 ± 1 and 3259 ± 5 Ma (Kohler and Anhaeusser, 2002).

South of the Inyoka Fault, the Fig Tree Group is divided into the Mapepe and the Auber Villiers Formations, which are also separated by a regional thrust fault (Lowe, 1999; Lowe et al., 1999, 2012). The sediments of the Mapepe Formation were deposited under conditions ranging from deep to shallow water and are characterized by quartz-poor siliciclastic, volcaniclastic, and chemical sediment (Heinrichs, 1980; Nocita, 1989; Nocita and Lowe, 1990; Lowe and Nocita, 1999). The Auber Villiers Formation consists of dacitic, plagioclase-phyric volcaniclastic conglomerate, breccia, and sandstone and displays a faulted contact with structurally underlying rocks of the Mapepe

Formation. The Auber Villiers Formation contains zircons of 3256 ± 4 Ma (Kröner et al., 1991) and 3253 ± 3 Ma (Byerly et al., 1996) and appears to underlie, perhaps conformably, sedimentary rocks of the Moodies Group (Lowe and Byerly, 1999).

In general, sediments of the Mapepe Formation in the southern Fig Tree Group were sourced from uplifts of the Onverwacht Group and from penecontemporaneous dacitic to rhyolitic volcanic rocks (Heinrichs, 1980; Nocita, 1989; Toulkeridis et al., 1998; Lowe and Nocita, 1999; Hofmann, 2005). The role of plutonic sources in Fig Tree sedimentation is uncertain. Over most of the studied BGB, rare microcline occurs in Fig Tree Group rocks but unambiguous plutonic pebbles and other components from deep-seated rocks are absent (Nocita, 1989; Lowe and Nocita, 1999) or sparse (Heinrichs, 1980; Hofmann, 2005).

Due to the fragmented character of the rocks of the Mapepe Formation, lithostratigraphic marker beds or datable ash beds are essential to the reconstruction of the Mapepe depositional system. Two excellent regional marker beds are the S2 and S3 spherule layers, which formed as condensates from rock-vapor plumes generated by large meteorite impacts (Lowe and Byerly, 1986; Lowe et al., 2003). These layers provide a firm basis for correlation among the structural blocks in which they occur. The S2 spherule bed at the base of the Mapepe Formation was deposited at ~3.26 Ga and the S3 spherule bed was deposited at ~3.24 Ga (Lowe et al., 2003). However, not all structural belts contain these spherule beds, other identifiable marker horizons, or datable ash beds, causing problems in assessing the stratigraphic relationships among many belts.

Lowe and Nocita (1999) reconstructed the depositional history of the Mapepe Formation, dividing the evolution in the west-central part of the BGB, including the EBV area, into three stages. During early Mapepe sedimentation, fine-grained and often iron-rich sediments, including thick units of BIF, were deposited in an extensive, relatively deep-water basin(s). During middle Mapepe time, shallow water sediments were deposited along an elongate, northeast-trending zone of uplift and erosion, termed the Proto-Inyoka Zone by Heinrichs and Reimer (1977). Middle and late Mapepe time was characterized by more continuous and widespread uplift and the formation of prograding fold-and-thrust belts flanked by two northeast-trending foreland basins. The East-Central Domain (ECD, Fig. 2), where the BARB4 and BARB5 drill cores were taken, represents the area of the proposed southeastern basin (see Fig. 18 in Lowe and Nocita, 1999). Here, a decrease in number, thickness, and grain size of sediments from the south-east to the north-west was taken to imply that sediments were sourced mainly from the southeast (Heinrichs, 1980; Lowe, 1999). Yet, the actual relationship of the numerous present-day structural belts remains unclear due to a paucity of marker horizons and geochronologic correlation.

The basal Mapepe Formation in the WCD has been dated at 3258 ± 3 Ma (Byerly et al., 1996) in the southeast and 3243 ± 4 Ma in outcrops immediately south of the Inyoka Fault (Kröner et al., 1991). Within the EBV area, Kröner et al. (1991) and Byerly et al. (1996) dated a dacitic tuff that stratigraphically overlies the top of the BARB5 core by about 20 m. It yielded a depositional age of 3227 ± 5 Ma and xenocryst ages or detrital zircon populations of 3281 ± 4 and 3484 ± 4 Ma.

3. Stratigraphy and sedimentology of the BARB4 and BARB5 ICDP drill cores

The ICDP-supported Barberton Drilling Project cored five sites in the BGB in order to investigate Archean surface conditions and crustal evolution. Two of the drill cores targeted sedimentary rocks of the Mapepe Formation (Figs. 2 and 3): the 540-m-long BARB4 drill core (25°54′24.09″S, 31°05′48.15″E) and the 760-m-long BARB5 drill core (25°54′26.49″S 31°03′31.41″E, azimuth 110°, dip 45°). Both cores were subdivided into several stratigraphic units (Fig. 3).

The stratigraphy of the BARB4 drill core, taken from the Manzimnyama Syncline (MS) structural belt (Fig. 2), was studied by Zentner (2014). The core penetrated at the base serpentinized komatiite and a thin chert of the Mendon Formation of the Onverwacht Group and, above, deep-water siliciclastic sandstone, BIF, banded ferruginous chert (BFC), and mudstone of the Mapepe Formation (Figs. 3A and 4A–D). The contact between the Onverwacht komatiites and overlying Fig Tree sedimentary rocks is disrupted by faults in the core that have severely attenuated the chert section at the top of the Onverwacht Group compared to nearby, unfaulted areas. The S2 spherule bed, which regionally marks the Onverwacht to Fig Tree contact, is absent in the BARB4 drill core.

Mapepe rocks in the BARB4 core are divided into five informal members, generally following subdivisions by Heinrichs (1980). The lower part of the sedimentary sequence, from 444 to 431 m core depth, is represented by mudstone and banded chert of the Loenen member that contain abundant fractures consistent with the inferred faulting (Fig. 3A). This is overlain from 431 m to 360 m core depth by mainly BFC, which we informally define here as the Schoonoord member, and from 360 m to 230 m by banded iron formation of the Lower Manzimnyama Jaspilite member. Both of these iron-rich intervals include minor chert-plate conglomerate and mudstone. The top ~220 m of the core consist of the Gelegela Grit member composed of coarse-grained, thick- to thin-bedded, lithic sandstone, and minor mudstone interpreted by Zentner (2014) to represent turbidites. In outcrop, the turbidite section is 350 m thick and succeeded by > 100 m of BIF of the Upper Manzimnyama Jaspilite member, the top of which is not exposed. Overall, the entire sedimentary sequence shows features consistent with deposition in a subaqueous below-wavebase and probably deep-water setting throughout Fig Tree sedimentation (Zentner, 2014).

The 760-m-long BARB5 drill core, which reflects approximately 400 m of stratigraphic section, was drilled in the EBV structural belt and exposes a sequence of siliciclastic, volcaniclastic, and orthochemical sedimentary rocks of the Mapepe Formation (Figs. 3B and 4E–H) (Heinrichs, 1980; Lowe and Nocita, 1999; Drabon, 2018). The stratigraphy and sedimentology of the EBV area is described in detail by Drabon (2018) but has also been discussed by Lowe and Nocita (1999) and Heinrichs (1980).

Drabon (2018) divided the Mapepe Formation in the BARB5 core into five informal lithologic members, termed members 1 through 5 from base to top. Member 1 is predominantly composed of 200 m of dark gray, maroon-weathering mudstone. At the base of the sequence (in outcrop and not penetrated by the core), silicified Mapepe sedimentary units, totaling about 3 m thick, include gray chert and BFC. They rest on spherule bed S2, which regionally marks the base of the Fig Tree Group. These are included in member 1. Towards the middle of member 1, thin, fine-grained sandstone beds interbedded with mudstone were deposited by weak turbidity currents. Overall, member 1 was deposited below wave-base in a deep-water environment. Locally, the mudstone shows soft-sediment folding and flowage, possible evidence of deposition on or near a slope. At 512 m core depth within member 1, the core penetrated the meteorite-impact-generated S3 spherule bed (Koeberl et al., 2015; Mohr-Westheide et al., 2015; Fritz et al., 2016; Schulz et al., 2017) that is overlain and underlain by mudstone, iron-rich mudstone, and minor jaspilite, all of which are parts of a complexly folded mass-transport deposit (Drabon, 2018). S3 is also present in surface outcrop, where it is part of member 2, a unit of interlaminated fine-grained sandstone, siltstone, and mudstone. The rocks in outcrop show abundant large, sweeping low-angle cross-stratification, wedging sets, and pinchouts. Member 2 reflects a shoaling-upward trend from the basinal sequence of member 1 to a more current- and/or wave-dominated shelfal setting. The sand-dominated rocks of member 3, which occur from 390 to 260 m in the core, show an increase in grain size and evidence for deposition by tidal processes. In member 4, pale green litharenite from 260 m to 95 m core depth marks an abrupt influx of dacitic volcaniclastic debris. The tuffaceous deposits include some chert intra-clast conglomerate and show abundant cross-lamination and soft-sediment deformation. This section marks the

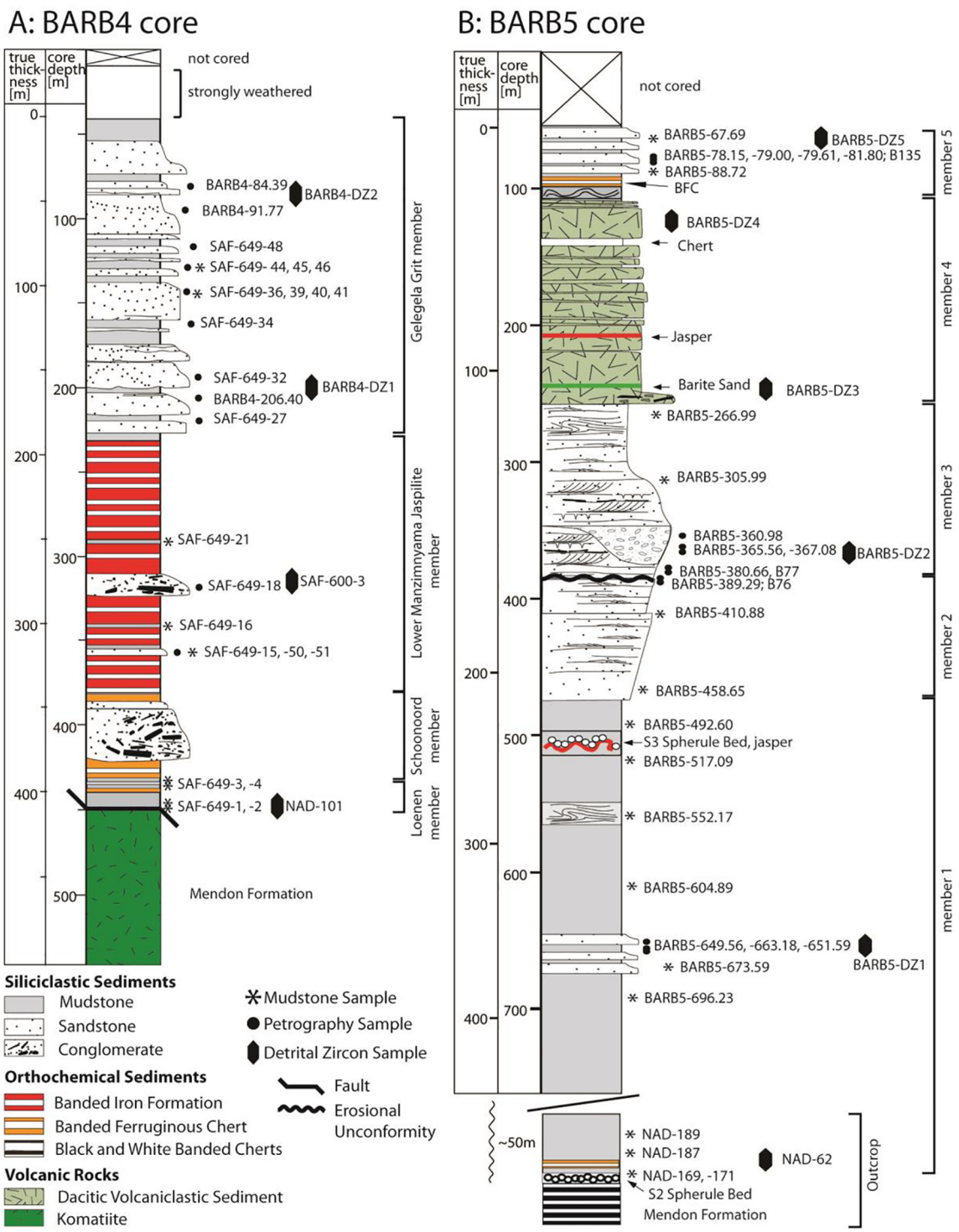

Fig. 3. Stratigraphy and sample locations of the [A] BARB4 (Zentner, 2014) and [B] BARB5 drill cores. Each core was subdivided into distinct units based on lithology and provenance. See Fig. 2 for drilling locations within the MS and EBV. Note that the S3 spherule bed at 512 m core depth in the BARB5 drill core is incorporated in a mass transport deposit.

initiation of Fig Tree dacitic volcanism in the EBV. Chert, barite, and jaspilite in outcropping parts of member 4 have been interpreted as a shallow-water bank association (Lowe and Nocita, 1999; Drabon, 2018) and mark the top of the upward-shoaling cycle that began with basinal mudstone sedimentation in the lower Mapepe Formation. In member 5, the sequence is capped by a return to deposition of mudstone and sandstone by turbidity currents and debris flows under deep-water conditions. Member 5 strata are only exposed in the BARB5 drill core above 95 m core depth and are mostly covered by a forestry plantation in outcrop.

4. Methodology

Samples were collected from the BARB4 and BARB5 drill cores for petrographic and geochemical analysis as well as detrital zircon geochronology (Fig. 3, supplementary material). Sandstone samples were point-counted using the Gazzi-Dickinson method with a minimum of 300 grains per thin section (Ingersoll et al., 1984). Mudstone samples

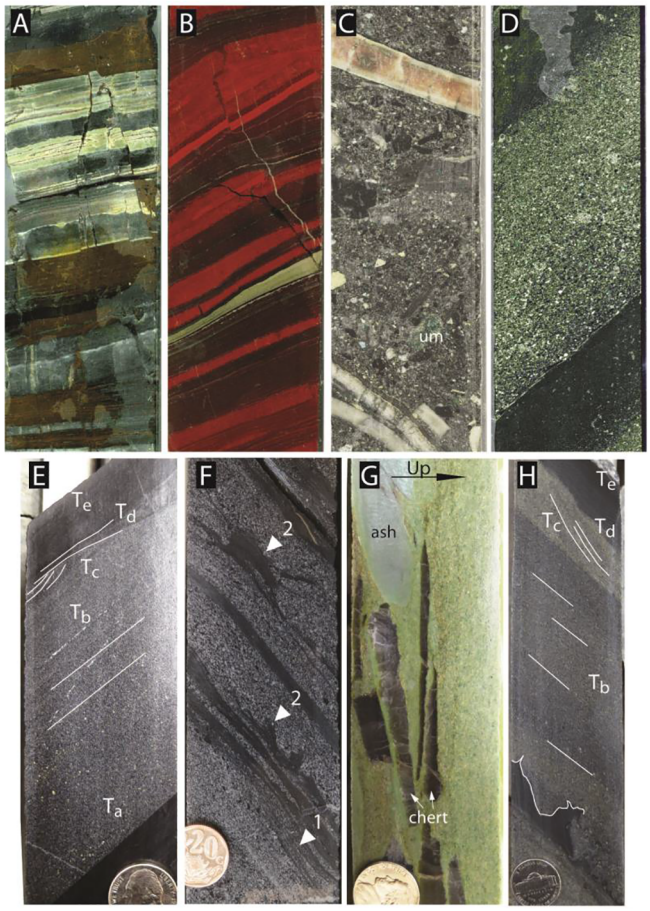

Fig. 4. Photographs of drill cores BARB4 [A–D] and BARB5 [E–H]. Drill cores are 4.5 cm in diameter. [A] Banded ferruginous chert at 409 m core depth (Schoonoord member). [B] Banded iron formation at 349 m core depth (Lower Manzimnyama Jaspilite member). [C] Conglomerate with translucent chert, white chert, ferruginous chert, carbonaceous chert and green silicified ultramafic clasts (um) at 321 m core depth (Lower Manzimnyama Jaspilite member). [D] Thin turbidite at 129 m core depth (Gelegela Grit member). [E] Turbiditic sandstone and mudstone at 661 m core depth (member 1). [F] Inter-tidal chertarenite with mud laminations (1) and mud clasts (2) at 360 m core depth (member 3). [G] Platy, angular chert clasts and rounded silicified ash clast in a matrix of dacitic tuffaceous debris at 161 m core depth (member 4). [H] Turbiditic sandstone with $T_{b\text{-}e}$ divisions after Bouma (1962) at 90 m core depth (member 5).

were analyzed for major, trace, and rare earth elements by XRF and ICP-MS at the GeoAnalytical Lab at Washington State University (supplementary material).

Zircon grains were extracted from 10 sandstone samples (2–6 kg) using standard size, hydrodynamic, and heavy-mineral separation techniques at Stanford University. Samples were crushed with a jaw crusher into rock chips and fed into a disk grinder to grind to medium-grained sand size. Light and heavy mineral fractions were separated utilizing a Gemini table. Following this, the magnetic minerals were removed from the heavy fraction utilizing a Frantz isodynamic magnetic separator. The residual minerals were separated using a heavy liquid (methylene iodide) to remove any remaining minerals less dense than 3.32 g/cm^3. Residual minerals typically contained > 99% pyrite and < 1% zircon. Zircon grains were hand-picked under a standard microscope and mounted onto 1 in. epoxy mounts together with Sri Lanka (563.5 ± 2.3 Ma), FC-1 (1099.0 ± 0.6 Ma), R33 (419.3 ± 0.4 Ma) and OG1 (3465.4 ± 0.6 Ma) zircon standards and then polished. The results are reported in the supplementary material.

$^{206}Pb/^{207}Pb$ ages were measured by Laser-Ablation Inductively Coupled Plasma Mass Spectrometry (LA-ICP-MS) with a 20 µm spot diameter at the Arizona LaserChron Center using the techniques discussed in Gehrels et al. (2008) and Gehrels and Pecha (2014). Grains with ^{204}Pb > 600 counts, low $^{206}Pb/^{204}Pb$, poor precision, U abundance above 400 ppm, or concordance below 95% were excluded.

One sample (NAD-101) was analyzed using the Sensitive High-Resolution Ion Microprobe - Reverse Geometry (SHRIMP-RG) at Stanford University following the methods of Premo et al. (2008). AS3, MAD, and OG1 were run as standards. Data reduction was accomplished using SQUID and ISOPLOT (Ludwig, 2001, 2003). Ages were calculated using ^{204}Pb-corrected $^{207}Pb/^{206}Pb$ ratios and ^{204}Pb-corrected $^{206}Pb/^{238}U$ and $^{207}Pb/^{235}U$ concordia model ages. Grains with U abundance above 400 ppm or concordance below 90% were excluded.

The Kolmogorov-Smirnov (K-S) Test was applied to statistically determine if the detrital zircon samples represented different parent rock or grain populations (e.g., Press et al., 1997; Berry et al., 2001). The lower the *P*-value, the more likely the samples were drawn from different populations. *P* values larger than 0.05 indicate that samples are not statistically different at ≥95% confidence and were likely drawn from the same population. We compared each sample's age distribution with every other sample to assess the heterogeneity of the sandstone samples (Table 1).

5. Results

5.1. Petrography

Petrographic analysis of sandstones can aid in the identification of rock types exposed in the source area, especially if lithic grains reveal textural and compositional characteristics of potential source rocks (Dickinson and Suczek, 1979; Ingersoll et al., 1984; Dickinson, 1970, 1985). However, interpretations of modal sandstone analyses are biased by the differential susceptibility of source rocks to weathering (Hessler and Lowe, 2006) and, in the case of BGB sandstone, by extensive recrystallization and metasomatism (e.g., Duchac and Hanor, 1987; Toulkeridis et al., 1998; Hofmann, 2005). The sand grain populations are thus likely representative of only the most chemically and physically resistant components of the source rocks. Unless silicified, basaltic and komatiitic rocks break down readily into clays and solutes and are

Table 1
Results in "P"-values of the K-S Test. Samples in bold have a p-value > 0.05, suggesting with 95% confidence that the two populations are not statistically different. Data include uncertainty in the construction of the Cumulative Distribution Function (CDF). Samples NAD-101 and NAD-62 were excluded due to the low number of grains analyzed.

	BARB5-DZ1	BARB5-DZ2	BARB5-DZ4	BARB5-DZ5	SAF-600-3	BARB4-DZ1	BARB4-DZ2
BARB5-DZ1		0.000	0.000	0.000	0.002	**0.138**	0.000
BARB5-DZ2	0.000		0.000	0.000	0.000	0.000	0.000
BARB5-DZ4	0.000	0.000		0.000	0.000	0.000	0.000
BARB5-DZ5	0.000	0.000	0.000		0.000	0.000	0.000
SAF-600-3	0.002	0.000	0.000	0.000		**0.709**	**0.306**
BARB4-DZ1	**0.138**	0.000	0.000	0.000	**0.709**		**0.061**
BARB4-DZ2	0.000	0.000	0.000	0.000	**0.306**	**0.061**	

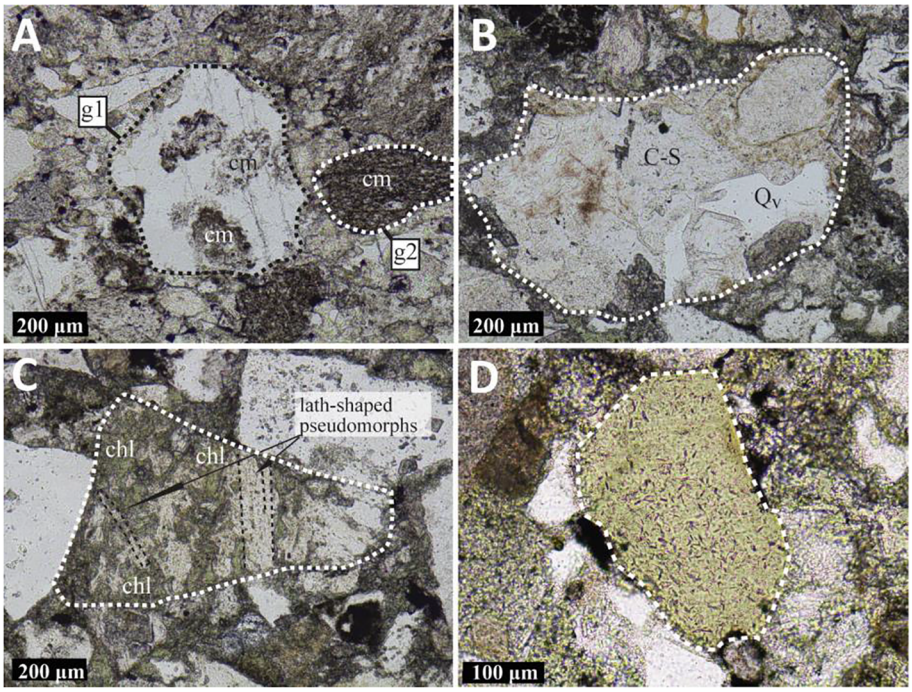

Fig. 5. Main grain types in Mapepe sandstones. [A] Carbonaceous chert grains: grain g1 is composed of clusters of carbonaceous material (cm) floating in pure chert; grain g2 is a pure carbonaceous chert grain with carbonaceous material dispersed throughout the grain. [B] Felsic lithic grain composed of a chert-sericite micromosaic (c-s) and skeletal β-quartz (Qv). [C] Intermediate to mafic lithic grain composed of bright-green chlorite (chl) and exhibiting lath-shaped pseudomorphs, probably representing plagioclase. [D] Chamosite grain with fine rutile laths from the upper part of the Gelegela Grit member in the BARB4 drill core.

thus underrepresented in the modal framework analysis of sandstone compared to felsic igneous rocks, chert, or quartz (Hessler and Lowe, 2006). Moreover, Hessler and Lowe (2006) show that an extreme loss of feldspar occurred during the source-to-sink evolution of sediments (including weathering, erosion, and transport of sediments) in the BGB. Partial and complete replacement of grains by secondary minerals, recrystallization, and incorporation of labile grains into a pseudo-matrix during post-depositional alteration and compaction additionally bias the petrographic results (Reimer, 1972; Condie et al., 1970; Lowe and Nocita, 1999; Heubeck and Lowe, 1999).

5.1.1. Grain types

All Mapepe sandstone units have undergone pervasive metasomatic alteration and most primary minerals except coarse-crystalline quartz, zircons, Fe-oxides, and spinels have been transformed into micromosaics of microquartz, phyllosilicates, and trace impurities. Lithic grains were identified by rare primary mineralogy and, more commonly, by textural and compositional features (Fig. 5), including the presence of pseudomorphs after phenocrysts or microlites. Monocrystalline quartz is generally unstrained and occurs in low proportions, averaging about 3% of the framework mode in BARB4 and 5% in BARB5 with highest values in BARB5-member 5 with 15%. Monocrystalline quartz commonly exhibits straight crystal faces and embayments indicative of volcanic β-quartz. Polycrystalline quartz grains composed of interlocking, > 35 µm quartz domains are also rare. They commonly show comb structures, systematic domain-size variations, and botryoidal textures consistent with an origin as vein- and cavity-fill quartz. Chert grains with quartz domains < 35 µm are common and range from compositionally pure chert (< 5% impurities) to chert containing varying trace amounts of carbonaceous matter (Fig. 5A), carbonate, hematite, and phyllosilicates. Feldspar is a minor component that, if present, is typically altered. Plagioclase is commonly partially to completely replaced by intergrown carbonate and sericite blades aligned along former cleavage and/or twin planes. The number of counted feldspar grains, including those replaced by secondary minerals but still clearly recognizable as altered plagioclase, thus represents a minimum value. No potassium feldspar or ferromagnesian minerals such as olivine, pyroxene, and amphibole were recognized.

Felsic to intermediate volcanic grains were identified by the presence of euhedral to subhedral crystals of volcanic quartz and euhedral to subhedral pseudomorphs after plagioclase in a matrix of intergrown chert, sericite, and carbonate, possibly representing recrystallized and carbonate-replaced volcanic glass (Fig. 5B). Mafic to ultramafic volcanic grains were identified by rare primary mineralogy, such as spinel, and, more commonly, by pseudomorphs after basaltic and komatiitic textures such as spinifex textures or plagioclase laths and microlites. These grains are now composed of intergrown chert, chlorite, (Cr-rich) sericite, and carbonate, indicating an Mg-, Fe-, and Cr-rich precursor (Fig. 5C). This type of alteration of komatiitic rocks can also be seen at the base of BARB4 where the komatiites are partially silicified and altered to chlorite, carbonate, talc, and biotite (Farber et al., 2016). Apart from these basaltic and komatiitic lithic grains, another type of chlorite-bearing grain-type was identified in sandstone in the upper part of the BARB4 core. These grains are composed of the mineral chamosite and have commonly undergone ductile deformation between more rigid grains (Fig. 5D, supplementary material). Chamosite is an iron-rich chlorite that occurs as an early-diagenetic mineral in sedimentary rocks and iron formation, including ooidal ironstone, deposited predominantly during the Proterozoic and Phanerozoic (Mücke, 2006; Dai and Chou, 2007; Sturesson et al., 2000), or by hydrothermal origin in association with magnetite (Rivas-Sanchez et al., 2006). Ooidal chamosite grains are thought to have formed by chemical precipitation of cryptocrystalline iron oxyhydroxides on available grains on the sea floor (Sturesson et al., 2000). Lithic grains composed of varying percentages of phyllosilicates in chert without any primary silicate minerals or recognizable textures could not be unambiguously classified but were likely formed by alteration of aluminum-bearing rocks, such as felsic volcanic rocks or mudstone. Accessory grains include rare biotite and muscovite as well as heavy minerals such as spinel, zircon, rutile, apatite, pyrite, and other opaque minerals.

All grains are angular and the sandstones are moderately to well sorted. The sandstones contain 22–43% by volume matrix and carbonate cement. The matrix is composed of intergrown minerals, including phyllosilicates, chert, chlorite, fine-grained carbonate and opaque grains. The matrix has, similar to lithic grains, experienced replacement and recrystallization. It was thus not possible to differentiate between epi-, ortho-, and pseudomatrix (Dickinson, 1970).

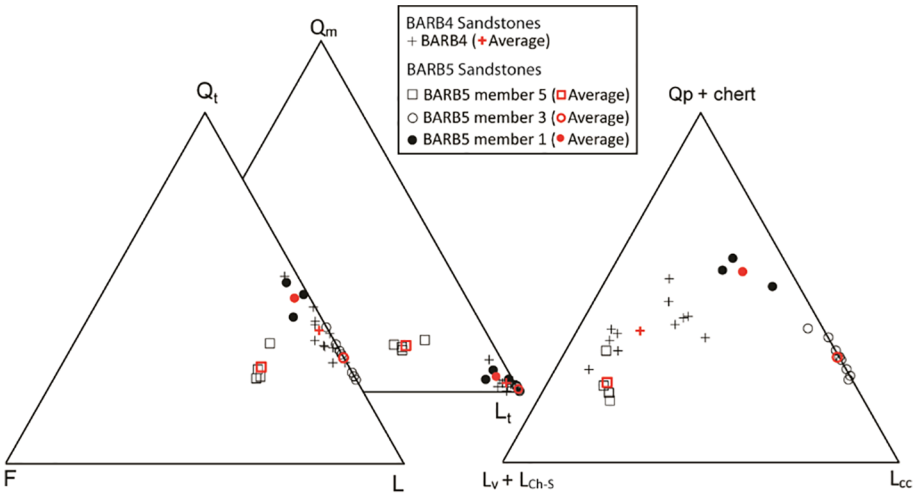

Fig. 6. Ternary plots of the modal framework grain compositions of medium-grained sandstones in the Mapepe Formation in the BARB4 and BARB5 cores. Abundance of feldspar represents a minimum estimate due to alteration. Q_t = total quartz; Q_m = monocrystalline quartz; F = feldspar; L = lithic grains; L_t = total lithic grains including polycrystalline quartz; Q_p = polycrystalline quartz; L_v = volcanic lithic grain; $L_{Ch\text{-}S}$ = chert-sericite lithic grain; Lcc = carbonaceous chert lithic grain.

5.1.2. Modal framework analysis

Eleven sandstone samples from BARB4 and fourteen from BARB5 were point-counted. In BARB4, sandstone intercalated with the Lower Manzimnyama Jaspilite and from the thick turbiditic sandstone unit at the top of the core, the Gelegela Grit member, display a relatively uniform framework mode with an average of 38.7% total quartz, 2.4% feldspars, and 58.9% lithic grains (Fig. 6). Monocrystalline quartz averages only 3.3%. The remainder of the counted quartz is composed of microcrystalline quartz (chert). The lithic grain proportion itself includes relatively pure microcrystalline quartz (38.2%), phyllosilicate-microquartz mixtures (average 44.3%), and carbonaceous chert (17.5%). Putative clusters in the BARB4 lithic grain population do not correlate with trends in the geochemistry, zircon geochronology, or stratigraphy. Some phyllosilicate-microquartz grains include chlorite, possibly suggesting the presence of altered mafic lithic grains. Above 160 m core depth, chamosite grains are present in the sandstone. The percentage of chamosite grains increases from an average of 2% of the framework mode below 193 m core depth to 22% above 155 m.

BARB5 includes three compositionally distinctive sandstone units with significantly different framework modes (Fig. 6). Turbiditic litharenite beds from 644 m to 668 m core depth (member 1), near the base of the cored section, contain 47.2% total quartz but only 4.5% monocrystalline quartz, 3.8% plagioclase, and 49.0% lithic grains (91.7% L_t). The chertarenite from 320 to 390 m core depth (member 3) is composed 99.2% total lithic grains of which 69.2% are sedimentary carbonaceous chert and 30% pure translucent chert, suggesting erosion into black and white banded cherts in the source. The volcaniclastic sandstone from 0 to 95 m core depth (member 5) contains abundant monocrystalline volcanic quartz (26.7%) and partially to completely replaced plagioclase (24.3%) derived from the directly underlying dacitic volcaniclastic sediments. The lithic grains are composed of 21.4% pure chert, 62.0% sericite-bearing grains, and 16.6% carbonaceous chert, representing grains derived from erosion of a recrystallized dacitic ash and banded and/or carbonaceous cherts. No chamosite grains were identified in the BARB5 drill core.

5.2. Mudstone geochemistry

Hessler and Lowe (2006) observed that immobile-element mudstone geochemistry provides the most accurate estimate of provenance because of the pervasive metasomatic alteration of BGB rocks. Numerous studies on the alteration of volcanic rocks in the BGB have shown that Al_2O_3, high field strength elements (HFSE), and REE were relatively immobile during post-depositional alteration and fluid migration (e.g., Pearce and Cann, 1973; MacGeehan and MacLean, 1980; Vennemann and Smith, 1999; Hessler and Lowe, 2006). We thus based the geochemical provenance analysis of the Mapepe Formation on Al_2O_3, specific trace elements (Th, Sc, Zr, Cr, and Ti) and the REE composition of mudstones.

5.2.1. BARB4 drill core

Fourteen mudstone samples were collected from the four stratigraphic units (Fig. 3) of the BARB4 core. Overall, SiO_2, TiO_2, and Al_2O_3 show values similar to average Archean mudstone (Fig. 7, Taylor and McLennan, 1985). In BARB4 mudstone, CaO, Na_2O, and Sr appear to be significantly depleted, up to two orders of magnitude less than mudstones of the average Archean upper crust. This depletion is consistent with post-depositional alteration trends seen throughout the BGB (e.g., Duchac and Hanor, 1987; Toulkeridis et al., 1998; Hofmann, 2005). K_2O and Rb are slightly enriched relative to the average Archean crust and mudstone. FeO* abundances are elevated in samples above 380 m core depth, reflecting the transition into the chemical sedimentation of BFC, BIF, and chamosite that characterize the middle and uppermost Mapepe Formation in the MS. It has been proposed that Cr adsorbs readily onto iron-hydroxides at neutral pH (Konhauser et al., 2011). While no co-variation between Cr and FeO* could be detected, we use Cr values in the Mapepe mudstone associated with iron formation only cautiously as a provenance indicator.

Mudstone samples from the Loenen and the Schoonoord members at the base of the sequence have a distinctly dacitic to rhyolitic provenance signature. Cr/Zr ratios decrease and Th/Sc ratios increase with differentiation in igneous rocks (Taylor and McLennan, 1995). For example, komatiites of the Mendon Formation have an average Cr/Zr ratio of 63 and a Th/Sc ratio of 0.1 (Decker et al., 2015) while rhyodacites from the Bien Venue Formation have a Cr/Zr ratio of 0.28 and Th/Sc ratio of 0.64 (Kohler and Anhaeusser, 2002). The values for Cr/Zr at the base of the core are relatively low (Fig. 8), ranging from 0.2 to 0.5, and relatively high for Th/Sc, ranging from 0.8 to 5.0, indicating a highly fractionated source terrane, with the exception of sample SAF 649-3 which has a more mixed provenance signature with Th/Sc = 0.6 and Cr/Zr = 6.6. However, the geochemistry suggests that sample SAF-649-3 was part of the Lower Manzimnyama Jaspilite member, not the Schoonoord member, and was juxtaposed by faulting. The average Th/Sc ratio of 2.1 is above the average of post-Archean mudstones of 1.0 (Taylor and McLennan, 1995). The samples plot in the La_N/Yb_N vs Th/Sc diagram towards granitic/rhyolitic compositions, similar to those in the Bien Venue Formation and the Auber Villiers Formation of the Fig Tree Group in more northern and northeastern parts of the BGB, and the 3.55–3.51 Ga Theespruit Formation of the lower Onverwacht Group (Fig. 9). Also in agreement with a highly fractionated rhyolitic/granitic source, the mudstones show high ΣREE values (ΣREE = 188 ppm), a strong LREE enrichment (La_N/Sm_N = 3.96), and a relatively flat HREE

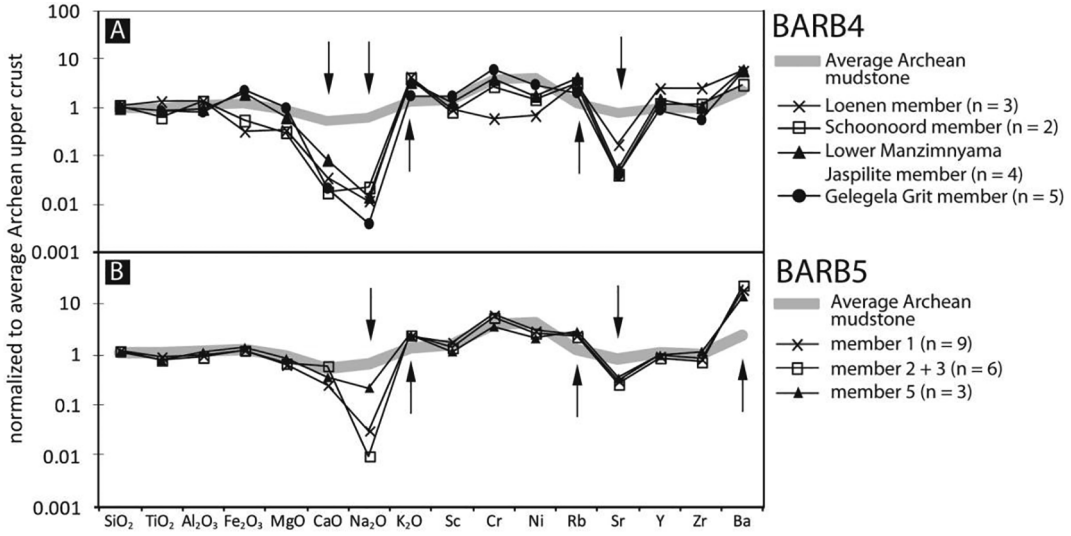

Fig. 7. Major and trace element analyses of mudstone of the Mapepe Formation in cores BARB4 (A) and BARB5 (B) normalized to the average Archean upper crust (Taylor and McLennan, 1985). Arrows indicate depletion (down) and enrichment (up) pattern relative to the average Archean upper crust. Samples from outcrop were excluded as they were affected by modern weathering.

pattern (Gd_N/Yb_N = 1.41). They lack the steep HREE pattern typical for TTGs in the BGB (Gd_N/Yb_N = 3.04, Kleinhanns et al., 2003) or of dacitic volcanic rocks in the BARB5 drill core (La_N/Sm_N = 4.4; Gd_N/Yb_N = 2.1) but more closely resemble REE pattern of rhyolites and rhyodacites in the Bien Venue and Theespruit Formations (Fig. 10C).

Higher in the BARB4 section, mudstone composition from the Lower Manzimnyama Jaspilite and Gelegela Grit members is consistent with a strong influence of basaltic and komatiitic sources. In the Lower Manzimnyama Jaspilite, the average Th/Sc ratio of 0.6 suggests a mixed mafic and felsic provenance. In comparison, the average Archean mafic crust displays a value of 0.02 while the average upper continental crust shows a value of 1. The REE pattern is in agreement with either a mixed felsic to ultramafic source or an intermediate source (Fig. 10). The LREE display a less fractionated pattern compared to the lower part of the BARB4 core, with La_N/Yb_N = 5.1 and Gd_N/Yb_N = 1.3, also indicating on average a less differentiated source terrane than samples from the Loenen and the Schoonoord members. Comparing the La_N/Yb_N vs. Th/Sc geochemical signatures to those of potential source rocks within the BGB, the mudstone samples plot as a mixture of felsic (rhyolitic and dacitic) and mafic (basaltic and komatiitic) source rocks (Fig. 9). Other geochemical provenance indicators (such as Cr and Fe) within the Gelegela Grit member may have been severely affected by the presence of chamosite grains. The trace element and REE geochemistry of chamosite is determined by the geochemistry of the fluid from which it precipitated, specifically the abundance of phosphate, which is likely to have been the carrier phase for the REE (Sturesson et al., 2000). Additionally, Cr^{3+} absorption onto ferric iron hydroxide (Konhauser et al., 2011) may have contributed to the elevated Cr abundance above 160 m core depth (Fig. 8A). A detailed geochemical study of the chamosite would be necessary to fully quantify its possible influence on the geochemical provenance signature.

5.2.2. *BARB5 drill core*

Thirteen mudstone samples from the BARB5 core and four outcrop mudstone samples from the base of the sequence that was not penetrated by the BARB5 drill core were analyzed for provenance (see supplementary material). BARB5 samples show compositions that are overall similar to that of the average Archean mudstone (Fig. 7). FeO and MgO values are lower than in BARB4 and comparable to the Archean upper crust, suggesting that they were not introduced into the section by precipitation of iron formation or by a source terrane unusually rich in basaltic and komatiitic source rocks. Similar to BARB4, K and Rb values are enriched and Na_2O and Sr appear significantly depleted, again suggesting post-depositional element mobility. Ba abundances (2548–8020 ppm) are elevated, 3.5 times higher than in BARB4 and an order of magnitude higher than those in the average Archean crust, reflecting precipitation of barite in the depositional system. Beds of nearly pure detrital as well as precipitative barite are widespread in the EBV (Heinrichs and Reimer, 1977; Lowe and Nocita, 1999; Drabon, 2018; Reimer, 1980). Ba-rich illite (Toulkeridis et al., 1998) and Ba-rich feldspars are also present.

Mudstone geochemistry reveals a consistent mix of felsic and mafic

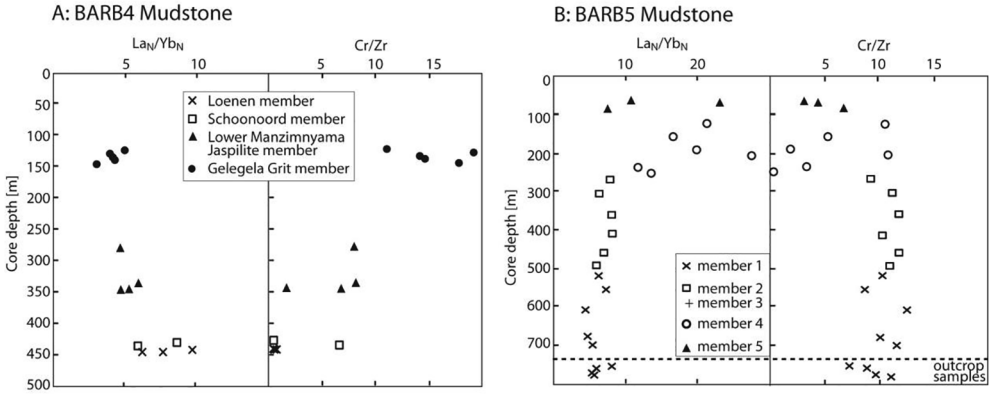

Fig. 8. La_N/Yb_N and Cr/Zr provenance plots of mudstones from the BARB4 and BARB5 drill cores. [A] BARB4 mudstones display upward-decreasing La_N/Yb_N and increasing Cr/Zr ratios, indicating an increasingly mafic source terrane and/or the influence of Cr^{3+} absorption onto ferric iron hydroxides. [B] BARB5 mudstones display an increasing La_N/Yb_N and a decreasing Cr/Zr ratio indicating an increasingly dacitic source terrane. Values from member 4 in the BARB5 drill core are from pure tuff samples and were taken from Galić (2015). REE were normalized to chondrite (Taylor and McLennan, 1985).

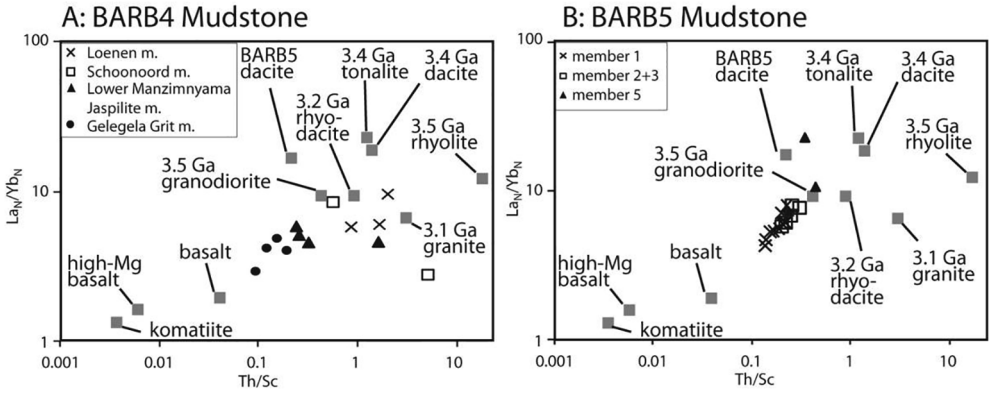

Fig. 9. Comparison of provenance-sensitive immobile element ratios La_N/Yb_N and Th/Sc in mudstone samples against possible source rocks within the BGB. [A] Basal rocks of BARB4 (Loenen and Schoonoord members) tend towards higher Th/Sc ratios indicating a more rhyolitic provenance. The Lower Manzimnyama Jaspilite and Gelegela Grit members plot in between mafic and felsic source rock compositions. [B] BARB5 mudstone samples of members 1, 2 and 3 plot in between basaltic to komatiitic and a felsic provenance. Sample from member 5 (triangles) have elevated La_N/Yb_N ratios, plotting towards the composition of the BARB5 dacites. Abbreviations within Figure: 3.2 Ga rhyodacite = Bien Venue Formation volcanic rocks (n = 2; this study); 3.4 Ga dacite = H6 member of the Hooggenoeg Formation (n = 7; this study); 3.5 Ga rhyolite = Theespruit Formation volcanic rocks (n = 5; Kohler and Anhaeusser, 2002); 3.5 Ga granodiorite = Steynsdorp granodiorite (n = 2; Kleinhanns et al., 2003); 3.4 Ga tonalite = Theespruit and Stolzburg tonalite; 3.1 Ga granite = Stentor and Mpuluzi plutons (n = 2; Kleinhanns et al., 2003); komatiite = komatiite of the Komati Formation (n = 7; Lahaye et al., 1995); high-Mg basalt = high-Mg basalt of the Hooggenoeg Formation (n = 4; Hofmann, 2005); basalt = basalt of the Hooggenoeg Formation (n = 3; Hofmann, 2005).

source rocks from the base of the BARB5 core upward to 260 m core depth where the composition becomes abruptly more dacitic. The lower part of the section is characterized by a uniform provenance signature with little variability: Cr/Zr and La_N/Yb_N have uniform values at 10.6 and 5.3, respectively. Compared to possible source rocks within the BGB (Fig. 9), they plot as mafic-to-felsic mixtures similar to mudstones from the BARB4 drill core of the Lower Manzimnyama Jaspilite and the lower Gelegela Grit members. The Cr abundance (average 984 ppm) indicates a contribution by komatiitic source rocks. BARB5 sediments are dominated by dacitic volcaniclastic components above 260 m core depth (member 4). As seen in Fig. 10, a tuff sample from member 4 shows the steep REE pattern typical of dacitic rocks characterized by enriched LREE (La_N/Yb_N = 14.39–32.14) and steep HREE pattern (Gd_N/Yb_N = 3.19–3.87). Stratigraphically higher mudstone samples from member 5 are again characterized by an intermediate or a mixed mafic and felsic source. However, compared to mudstones from members 1, 2, and 3, the source appears more felsic because the Cr/Zr values are lower (average of 4.7), La_N/Yb_N values elevated (average of 19.83) and ΣREE values high (average of 129 ppm). Fig. 10B shows that the HREE pattern is relatively steep (Gd_N/Yb_N = 1.68–2.86), likely related to erosion and reworking of the underlying dacitic tuff rather than basaltic or rhyolitic source rocks which are characterized by flat HREE patterns (Fig. 10C–E). These findings support the inference that felsic volcaniclastic strata from the base of BARB4 and the top of BARB5 have different compositions: Basal BARB4 mudstone units (Loenen and Schoonoord members) show a predominantly rhyolitic geochemical signature, whereas member 5 mudstone on top of BARB5 shows a dacitic signature, consistent with the associated dacitic volcaniclastic rocks.

5.3. Detrital zircon geochronology

Zircon grains form most commonly in magmas with > 60% silica (Stevenson and Patchett, 1990; Nutman, 2001). Detrital zircon can thus be used as tracers for dacitic to rhyolitic rocks in the source terrane, but do not provide information about the type of felsic source rock (intrusive vs. extrusive) or information about outcropping mafic rocks.

Samples were collected throughout the drill cores and adjacent outcrop (see Figs. 3 and 11; supplementary material). In the MS, zircon grains from sample NAD-101 from the Loenen member in outcrop are predominantly euhedral and show a single age population with a weighted mean SHRIMP $^{206}Pb/^{207}Pb$ age of 22 zircon grains at 3277 ± 4 Ma. All other samples throughout the MS (core samples BARB4-DZ1, BARB4-DZ2, and outcrop sample SAF-600–3, approx. correlative to 320 m core depth) show mainly slightly rounded and subhedral to anhedral zircon grains and display a main zircon age cluster at 3.45 Ga. Minor clusters occur at 3.55 Ga and, for samples SAF-600–3 and BARB4-DZ2, at 3.29 Ga. These three samples are relatively homogenous and have *P* values from 0.709 to 0.061 (Table 1). Thus, all of these sediments could have been derived from the same source region. Due to the paucity of penecontemporaneous zircon grains, no reliable depositional ages could be calculated. However, Byerly (pers. commun.) dated zircon from the Lower Manzimnyama Jaspilite member at 3,260 ± 5 Ma but the exact stratigraphic location of the sample is not known.

EBV detrital zircon grains of samples NAD-62 from the Onverwacht-Fig Tree contact, BARB5-DZ1 from member 1, and BARB5-DZ2 from member 3 are mainly subhedral to anhedral and moderately rounded, indicating no or minor zircon abrasion during transport. Zircon grains from samples BARB5-DZ3 and -DZ4 from the dacitic volcaniclastic rocks of member 4 and BARB5-DZ5 from member 5 are, in contrast, euhedral prismatic to moderately rounded, indicating a mix of juvenile zircon grains and zircon grains that experienced more extensive sedimentary reworking. All detrital zircon grains are pink to maroon in color and representative CL images show oscillatory zoning typical for igneous zircon (Fig. 11C). Collectively, detrital zircon spectra from BARB5 show seven main age clusters (Fig. 11B) at 3.24 (BARB5-DZ4 and -DZ5), 3.25 (BARBB5-DZ2), 3.26 Ga (NAD-62), 3.29 (NAD-62, BARB5-DZ2, -DZ,3 and -DZ4), 3.45 (BARB5-DZ1, -DZ2, -DZ3, -DZ4, and -DZ5), and 3.55 Ga (BARB5-DZ3, -DZ4, and -DZ5). All samples from the EBV area are heterogeneous with $P = 0$ and likely reflect different source populations. Only a single unit appears comparable across the two drill cores: the Gelegela Grit member of BARB4, represented by sample BARB4-DZ1, and member 1 in BARB5, represented by sample BARB5-DZ1. Because the P-value of these two samples is 0.138, they could have been drawn from the same population. In general, the detrital age population of all samples from the MS, except from the Loenen member, show a notable similarity to BARB5-DZ1.

The sandstone units in both cores do not show any evidence for derivation from crystalline or metamorphic basement; we therefore only consider felsic volcanic rocks as possible sources. The age peaks of detrital zircon from sandstone units in the BARB4 and BARB5 drill cores (Fig. 11) coincide broadly with known major episodes of dacitic to rhyolitic volcanism in the BGB. The youngest detrital zircon age cluster at 3.26–3.22 Ga corresponds to dated Fig Tree felsic volcanic rocks (Armstrong et al., 1990; Kröner et al., 1991; Byerly et al., 1996). Mendon Formation-age zircon grains at 3.29 Ga are not represented by any known felsic magmatic source within the BGB or vicinity but have previously been reported in smaller quantities from tuffs in the Mendon Formation (Byerly et al., 1996; Decker et al., 2015) and are found as a major age peak in U-Pb detrital zircon analyses of sandstones

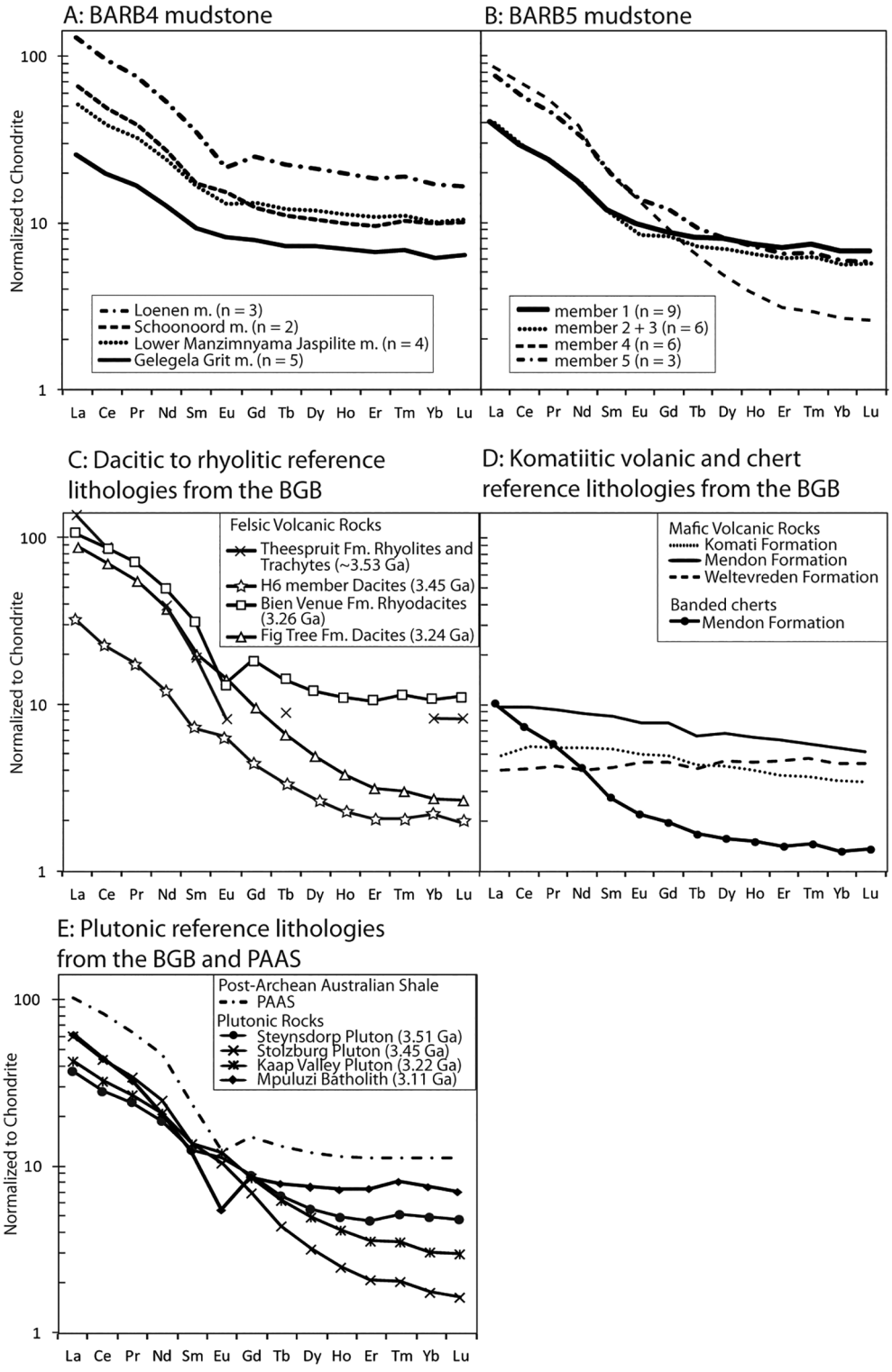

Fig. 10. Average REE normalized to chondrite from mudstone samples of [A] the BARB5 drill core, and [B] the BARB4 drill core. [C] Comparison to potential dacitic to rhyolitic extrusive source rocks within the BGB. Theespruit Formation felsic meta-volcaniclastic rocks (n = 5; Kohler and Anhaeusser, 2002); H6 member dacitic volcanic rocks (n = 8; this study); Fig Tree dacitic volcanic rocks (n = 1; this study); Bien Venue rhyodacites (n = 2; this study). [D] Comparison to potential basaltic and komatiitic volcanic source lithologies as well as cherts. Komati Formation (n = 8; Lahaye et al., 1995), Weltevreden Formation (n = 3; Lahaye et al., 1995); Mendon Formation (n = 3; Lahaye et al., 1995); Banded cherts of the Mendon Formation (n = 14; unpubl. data). [E] Comparison to potential intrusive source lithologies within the BGB and PAAS (Post-Archean Australian Shale). Steynsdorp granodiorite (n = 2; Kleinhanns et al., 2003); Stolzburg tonalite (n = 3; Kleinhanns et al., 2003; Hessler and Lowe, 2006); Kaap Valley Tonalite (n = 3; Kleinhanns et al., 2003; Hessler and Lowe, 2006); Mpuluzi Granite (n = 1; Kleinhanns et al., 2003).

throughout the BGB (Drabon et al., 2017). The volcanic source to these zircon grains may have been completely eroded or was located outside the present-day BGB. The 3.45 Ga cluster overlaps with crystallization ages of the felsic volcanic rocks of the H6 member of the Hooggenoeg Formation (Kröner and Todt, 1988; Armstrong et al., 1990; Kröner et al., 1991; Byerly et al., 1996). The 3.55 Ga ages correspond to crystallization ages of the Theespruit Formation felsic volcanic rocks (Kröner et al., 1996, 2016; Armstrong et al., 1990; Roerdink et al., 2016). Similar age peaks are also reported from the highly metamorphosed Dwalile Supracrustal Suite and the Luboya and Kubuta granulite-grade paragneisses in the AGC (Taylor et al., 2016; Van Schijndel et al., 2017).

6. Discussion

6.1. Alteration of rocks of the Mapepe Formation

Numerous factors including source-area composition, weathering,

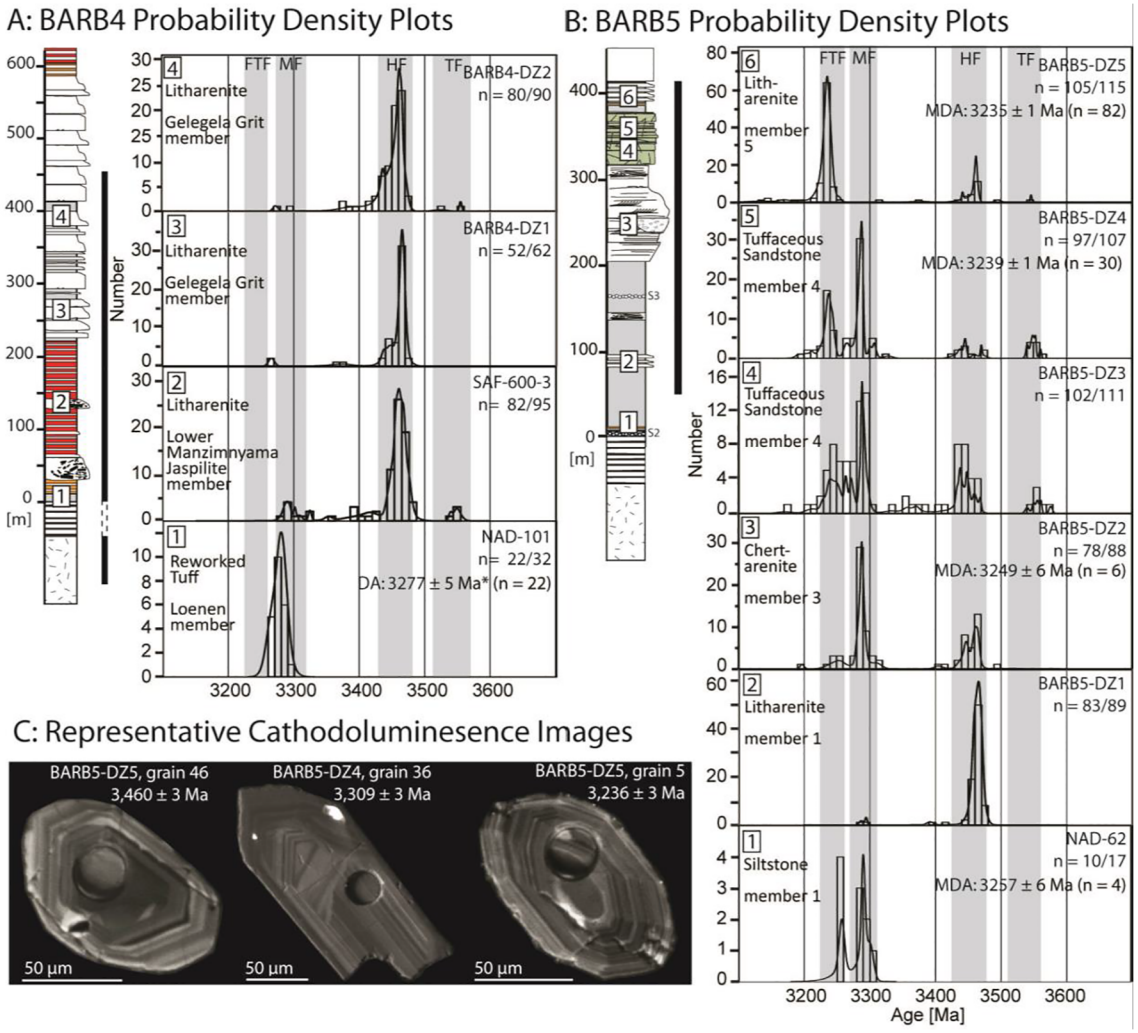

Fig. 11. [A and B] Probability density plots of detrital zircon analyses of sandstones from the [A] BARB4 and [B] BARB5 drill cores. Ages of potential dacitic to rhyolitic volcanic source rocks within the BGB are highlighted by gray bars. FTF = Fig Tree Formation volcanic rocks, MF = Mendon Formation volcanic rocks, HF = member H6 Hooggenoeg Formation volcanic rocks, TF = Theespruit Formation volcanic rocks. Maximum depositional ages (MDA) and depositional ages (DA) were calculated as weighted mean ages of youngest age clusters in Isoplot 3.75. Samples without calculated MDA do not contain enough young grains or exhibit no separate young age cluster. Sample marked by * was analyzed using a SHRIMP-RG, all other samples were analyzed using LA-ICP-MS. [C] Representative cathodoluminescence images of detrital zircon grains in the BGB showing oscillatory zoning typical for igneous zircons. Pits are from LA-ICP-MS analyses.

hydraulic sorting, diagenesis, and metasomatism can affect the composition of clastic sediments and sedimentary rocks. Similar to other areas within the BGB, the sedimentary rocks in the MS and EBV show evidence for severe alteration.

Petrographically, the effects of post-depositional alteration in the study area are evident by the recrystallization of most labile components, including most fine-grained lithic particles, glassy grains, and feldspars, into micromosaics of microquartz, phyllosilicates, carbonates, and trace impurities. Lithic grains commonly reveal their origin only by the presence of pseudomorphs after primary minerals, such as feldspar phenocrysts. The dacitic components include primary beta-quartz phenocrysts and partially altered biotite. These float in a matrix of chert-sericite ± finely disseminated carbonate, interpreted to represent recrystallized glass, fine-grained matrix, and/or labile lithic grains. Other indicators of post-depositional alteration in thin section include the presence of secondary euhedral pyrite and carbonate in the matrix (ankerite, dolomite, and siderite), formation of quartz and calcite veins, and alteration halos around detrital Cr-rich spinels.

K-metasomatism has been reported regionally from the BGB (e.g., Duchac and Hanor, 1987) and is supported here by sericitication of feldspars and lithic grains and K abundances in excess of those predicted from the composition of the likely source rocks. This is consistent with the analysis of carbonate within the EBV by Toulkeridis et al. (1998) who found that Sm-Nd, Rb-Sr, and U-Pb isotope systems of whole-rock carbonate samples were reset at 2.7 Ga, providing strong evidence for a major alteration event perturbing these isotopic systems at temperatures of at least 200 °C. They proposed that large-scale fluid movement caused secondary carbonatization, sericitization and silicification of the carbonates, resulting in addition of K, Rb, and loss of Sr.

BARB5 and BARB4 mudstone samples, as well as BGB rocks in general, show mobilization of mobile cations with small ionic radii such as Na and Ca. Na_2O abundances in both cores and CaO abundances in BARB4 are uniformly very low in comparison to plausible source rocks such as komatiite, basaltic komatiite, basalt, and the TTG intrusive equivalents to the dacitic to rhyolitic volcanic rocks (Lowe and Byerly, 1986; Hessler and Lowe, 2006; Hofmann and Harris, 2008). This depletion suggests post-depositional depletion of Na^+ and Ca^{2+}. CaO values are elevated in sedimentary rocks of BARB5, where carbonate is abundant as cement, carbonate grains, alteration products of feldspars, and carbonate veins. The inferred timing of carbonate formation with respect to other components of the rocks suggests that much of the carbonate is of diagenetic origin.

Many rocks of the Onverwacht Group have experienced silicification (Knauth and Lowe, 1978, 1999; Duchac, 1986; Duchac and Hanor, 1987; Lowe and Byerly, 1986). However, post-depositional silicification does not appear to have greatly affected the mudstone of the Mapepe Formation studied here. Mudstone shows average SiO_2 values of 63 wt.% for BARB4 and 67 wt.% for BARB5, comparable to PAAS (62 wt.% SiO_2). In the EBV area, silica abundances vary across different lithological units and are strongly elevated within carbonate-rich units, which show up to 60 wt.% SiO_2 (Toulkeridis et al., 1998) and the volcaniclastic rocks of member 4, which show up to 91 wt.% SiO_2 (Galić, 2015).

Weathering indices, such as the Chemical Index of Alteration (CIA, Nesbitt and Young, 1982), are common tools used to characterize the weathering regime and intensity of weathering reflected in a sedimentary sequence. However, the effects of mobile element depletion (especially Ca and Na), silicification, and K-addition raise serious doubts about the reliability of such indices for estimating the degree of weathering reflected by rocks of the Mapepe Formation in the study area.

6.2. Sediment sources of the Mapepe Formation

Sediments of the Mapepe Formation reflect erosion of supracrustal rocks similar to those making up underlying parts of the BGB. This was determined from (1) petrographic analysis that shows a predominance of grains derived from cherts and silicified rhyolitic, dacitic, basaltic, and komatiitic volcanic rocks; (2) the mixed komatiitic and basaltic to dacitic and rhyolitic geochemistry; and (3) the similarity of detrital zircon age clusters of different samples. The underlying Onverwacht Group is composed largely of basaltic and komatiitic volcanic rocks with at least two major intervals of felsic magmatism, one of Theespruit age at 3.51–3.55 Ga, and a second of Hooggenoeg age at approximately 3.45 Ga. In addition, detrital zircon samples throughout the BGB show indirect evidence for felsic volcanism at 3.29 Ga (Drabon et al., 2017). Deposition of banded chert occurred throughout accumulation of the Onverwacht sequence (Lowe, 1999). Besides erosion of the underlying Onverwacht Group, the MS and EBV sedimentary systems also recycled sediments of the Mapepe Formation. Various modes of chemical sedimentation were active throughout the deposition of the Mapepe Formation. They formed a variety of primary deposits that became sources of recycled detrital sediment when uplifted and eroded. Overall, the supracrustal rocks of the BGB form a lithologic suite identical to the combination of source rocks identified for the Mapepe Formation.

Some authors have proposed a sediment source from the AGC into the Mapepe sediments. For example, Hofmann (2005) reported a 200 m thick sequence of sedimentary rocks with a rhyolitic provenance signature at the base of the Mapepe Formation in the north-central Southern Domain. He proposed they were sourced from rhyolitic/granitic sources in the AGC because no such felsic sources had been identified within the BGB terrane. However, rhyolitic source rocks have been shown to occur in the BGB sequence. This includes rhyolitic volcanism during Fig Tree time, specifically volcanism represented by the reworked rhyolitic tuff from the 3277 Ma Loenen member at the base of the Mapepe Formation as well as rhyolitic and rhyodacitic volcanic rocks from the lower Fig Tree Group in the Auber Villiers Formation dated at 3256 ± 4 Ma (Kröner et al., 1991) and 3253 ± 3 Ma (Byerly et al., 1996) in the west-central BGB (Lowe and Byerly, 1999). Rhyodacitic rocks also occur in the Bien Venue Formation dated at 3259 ± 5 Ma and 3256 ± 1 (Kohler and Anhaeusser, 2002) 50–75 km to the northeast. There are also older rhyolitic sources from the Theespruit Formation within the basal Onverwacht Group. Thus, the rhyolitic provenance signature of Mapepe mudstones does not necessitate the AGC as a sediment source.

The composition and texture of sand grains in the Mapepe Formation also argues against a source from the AGC. The sand grains are angular, composed largely of lithic grains, and show no evidence of prolonged transport, recycling, or mixing with more diverse grain populations. The extreme paucity of coarse, monocrystalline quartz, other than that directly associated with quartz-phyric volcaniclastic rocks at the base of the BARB4 (Loenen member) and the dacitic volcaniclastic rocks at top of the BARB5 (members 4 and 5) cores, indicates that no coarse-crystalline metamorphic or plutonic rocks were exposed in the source area(s). This is supported by the virtual absence of potassium feldspar, coarsely crystalline plutonic rock fragments, and high-grade metamorphic rock fragments and minerals. Because TTG plutons had intruded at depth during earlier magmatic events, we conclude that erosion had not yet reached these deeper-seated plutonic rocks, which would have had an enormous potential to yield sand-sized sediment during exposure and weathering. This deep erosion into crystalline basement may have occurred later during deposition of the Moodies Group (Heubeck, 2019). These same features also argue against a deep-seated AGC source for these sediments. While some zircon age clusters of the Mapepe Formation overlap with age clusters of the highly metamorphosed Dwalile Supracrustal Suite and with those of the Luboya and Kubuta paragneisses in the AGC (Taylor et al., 2016; Van Schijndel et al., 2017), the compositional and textural immaturity of Mapepe sediments argues for a local origin, short distance of sediment transport, and rapid deposition. Thus, the sedimentary rocks do not provide evidence for a provenance linkage to the AGC.

Collectively, the characteristics of the sedimentary rocks in the Mapepe Formation argue that they represent first-cycle sediments that were derived from uplifts of supracrustal rocks of the Onverwacht and Fig Tree Groups as well as from penecontemporaneous dacitic to rhyolitic volcanism.

6.3. Diachronous onset of Mapepe sedimentation

Previous U-Pb dating of tuffs and tuffaceous sedimentary rocks has suggested a diachronous onset of Mapepe deposition (Byerly et al., 1996). Immediately south of the Inyoka Fault, a dacitic tuff sample from the base of the Mapepe Formation yielded a depositional age of 3243 ± 4 Ma (Kröner et al., 1991). Further to the south, the base of the Mapepe Formation is marked by the occurrence of the S2 spherule bed (Lowe et al., 2003) which has an age of ~3260 Ma based on an U-Pb zircon age of 3258 ± 3 Ma from a felsic tuff about 20 m above S2 (Byerly et al., 1996). The S2 spherule layer is also present within the EBV and provides an age constraint in agreement with the detrital zircon maximum depositional age of 3257 ± 6 Ma obtained from the base of the section in the EBV (NAD-62).

This trend of southward increasing age for the onset of Mapepe sedimentation appears to continue into the Manzimnyama Syncline. Sandstones of the Loenen member at the base of the formation represent only slightly reworked tuffaceous sediment derived from penecontemporaneous rhyolitic volcanic activity (Heinrichs, 1980) as indicated by (1) the abundance of felsic volcanic particles with up to 60% coarse volcanic ß-quartz, much of which exhibits straight crystal faces and embayments; (2) the single age peak of 3.277 ± 5 Ga (NAD-101) suggests that the volcaniclastic sediment was not mixed with older detrital zircon grains as is common for siliciclastic sediments throughout the BGB; and (3) the mudstone geochemistry shows a composition similar to known rhyolitic volcanic rocks throughout the BGB sequence. Additionally, the immaturity of the grains suggests that they do not represent material that experienced prolonged sedimentary transport or repeated recycling. Thus, while zircon crystallization can predate eruption for a few tens of thousands to millions of years (Crowley et al., 2007), the 17 Ma difference in age between the MDAs of the basal units in both synclines makes it reasonable to assume that Mapepe deposition in the MS occurred prior to deposition in the EBV.

In summary, the initiation of Mapepe sedimentation likely varied over 30 Ma, from as early as 3277 to 3243 Ma, across the BGB. Tectonic uplifts in the central BGB appear to have first formed in the southeast and successively progressed towards the northwest. Based on this

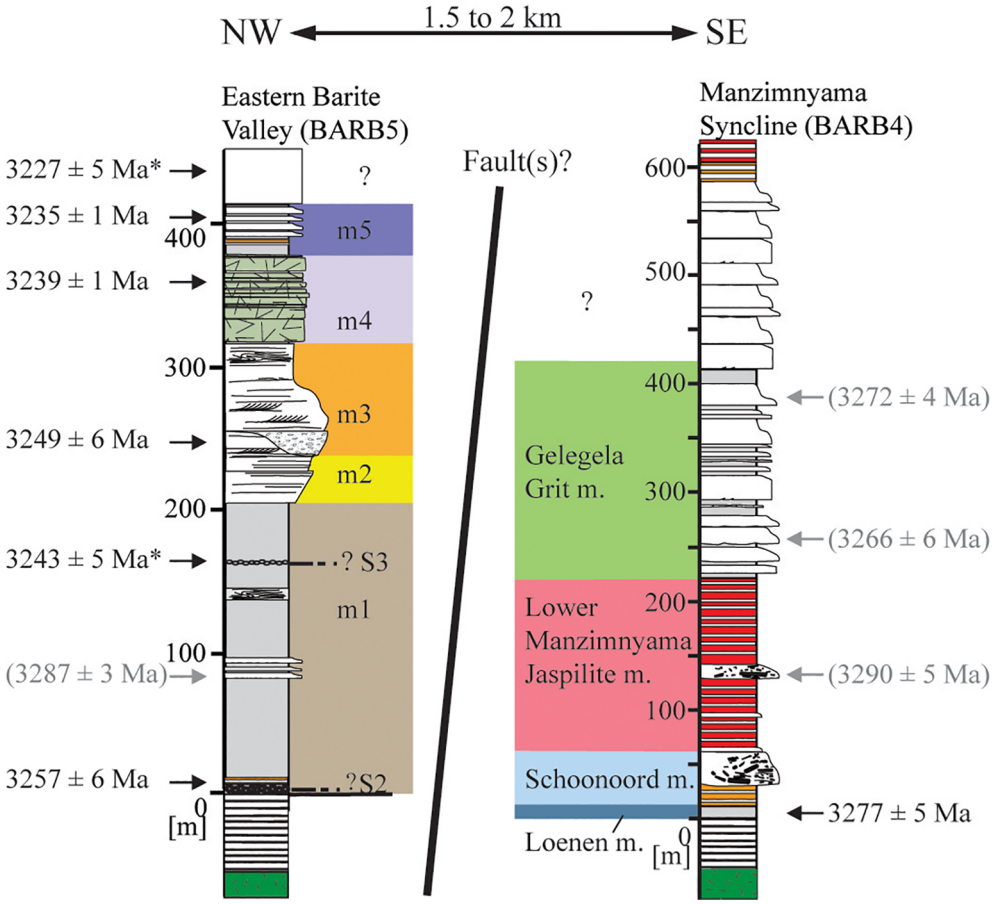

Fig. 12. Stratigraphic sections of the MS and EBV with lithologic units and maximum depositional ages based on detrital zircon analyses and depositional ages of tuff analyses. Zircon dated from the lower Manzimnyama Jaspilite member yield an age of 3260 ± 5 Ma (Byerly, pers. commun.). The ages in parentheses are likely older than the true depositional age or were derived from too few zircon analyses to determine a meaningful age. Because of the differences in depositional settings and lithology, no unequivocal correlation between the two sections is possible. Despite this uncertainty, dated sections of the lower MS appear to have significantly greater depositional ages than any units in the EBV. Available provenance data is consistent with the Lower Manzimnyama Jaspilite and the Gelegela Grit member in the MS section being approximately time-correlative with member 1 in the EBV. The top parts of the EBV and the MS sections, marked with a "?" in the columns, were not analyzed in this study. For legend refer to Fig. 2. Note the change in scale. m = member. Samples marked with * are from Kröner et al. (1991) and Byerly et al. (1996). Measured section of the MS is from Zentner (2014).

diachroneity of the onset of sedimentation, the structural belts of the Mapepe Formation cannot be assumed time-correlative.

6.4. Evolution of the Mapepe Formation

6.4.1. The Manzimnyama Syncline

The composition of Mapepe sedimentary rocks in the MS shows an up-section change from rhyolitic to more basaltic and komatiitic source rocks while being continuously deposited in relatively deep water (Figs. 8, 9, 12, 13). The relatively thin Loenen and Schoonoord members have a distinctly rhyolitic provenance. Above these basal sediments, Mapepe rocks in the Lower Manzimnyama Jaspilite and the Gelegela Grit members show a more basaltic to komatiitic source based on their geochemistry. This komatiitic to basaltic component is now underrepresented in the sandstones because komatiite and basalt weather readily to clay-sized detritus or solutes (Lowe and Byerly, 1986; Hessler and Lowe, 2006). No basaltic or komatiitic volcanism is known during Mapepe time, indicating that the sedimentary rocks reflect erosion into komatiitic rocks of the Onverwacht Group in the source area. The framework mode of the BARB4 sandstone in the Lower Manzimnyama Jaspilite and the Gelegela Grit members represents a composite of common silicified volcanic and sedimentary BGB rocks and does not show the distinct variability of BARB5 sedimentary rocks (Fig. 6). Overall, the sediments were locally derived as inferred from the angularity of grains and the abundance of labile lithic grains.

Chemical precipitation of iron hydroxides in the water column played a significant role during the deposition of Mapepe sediments in the MS. From about 360–230 m core depth in BARB4, the Lower Manzimnyama Jaspilite member is dominated by BIF. Coinciding with the onset of BIF deposition, the mudstone samples display high FeO* abundances, averaging about 15.6 wt.%. These mudstones are intercalated with hematitic and sideritic BIF, suggesting that the precipitation of Fe and mudstone deposition occurred closely in time and perhaps commonly overlapped. Many mudstone beds interbedded with sandstones in the lower part of the Gelegela Grit member in the BARB4 core are not directly associated with BIF or chamosite, but still show high iron abundances. This suggests that environmental conditions for iron precipitation persisted during mud and sand deposition. About half way through the sand-rich Gelegela Grit member, chamosite grains appear as abundant components of the sandstones, comprising up to 22% of the framework mode (Fig. 5D). This is reflected in the accompanying increase in FeO*, up to 35 wt.%, in the interlayered mudstone. Chamosite has rarely been described from Archean strata, but Harrington (2017) reported primary sedimentary chamosite in the middle to upper Mapepe Formation in the structural belt to the southeast of the MS, the Paulus Syncline. While the Paulus Syncline has a different detrital zircon signature and is thus unlikely to be a direct source, or to lie along the same sediment transport fairway as the MS sediments, the occurrence of sedimentary chamosite in the BGB suggests that it may have formed in adjacent settings and was then eroded and transported by turbidity currents into deeper water. This chamosite-bearing turbidite section is 220 m thick in the BARB4 core but extends to a full thickness of 350 m in outcrop where the turbiditic sandstones are overlain by another > 100 m-thick section of BIF, the top of which is not exposed. In summary, throughout the deposition of the sedimentary rocks of the Mapepe Formation in the MS, deposition occurred in relatively deep water and was characterized by abundant iron precipitation.

6.4.2. The Eastern Barite Valley area

Mapepe sedimentary rocks in the EBV, including core BARB5, display a discrete temporal evolution in sandstone petrography, mudstone

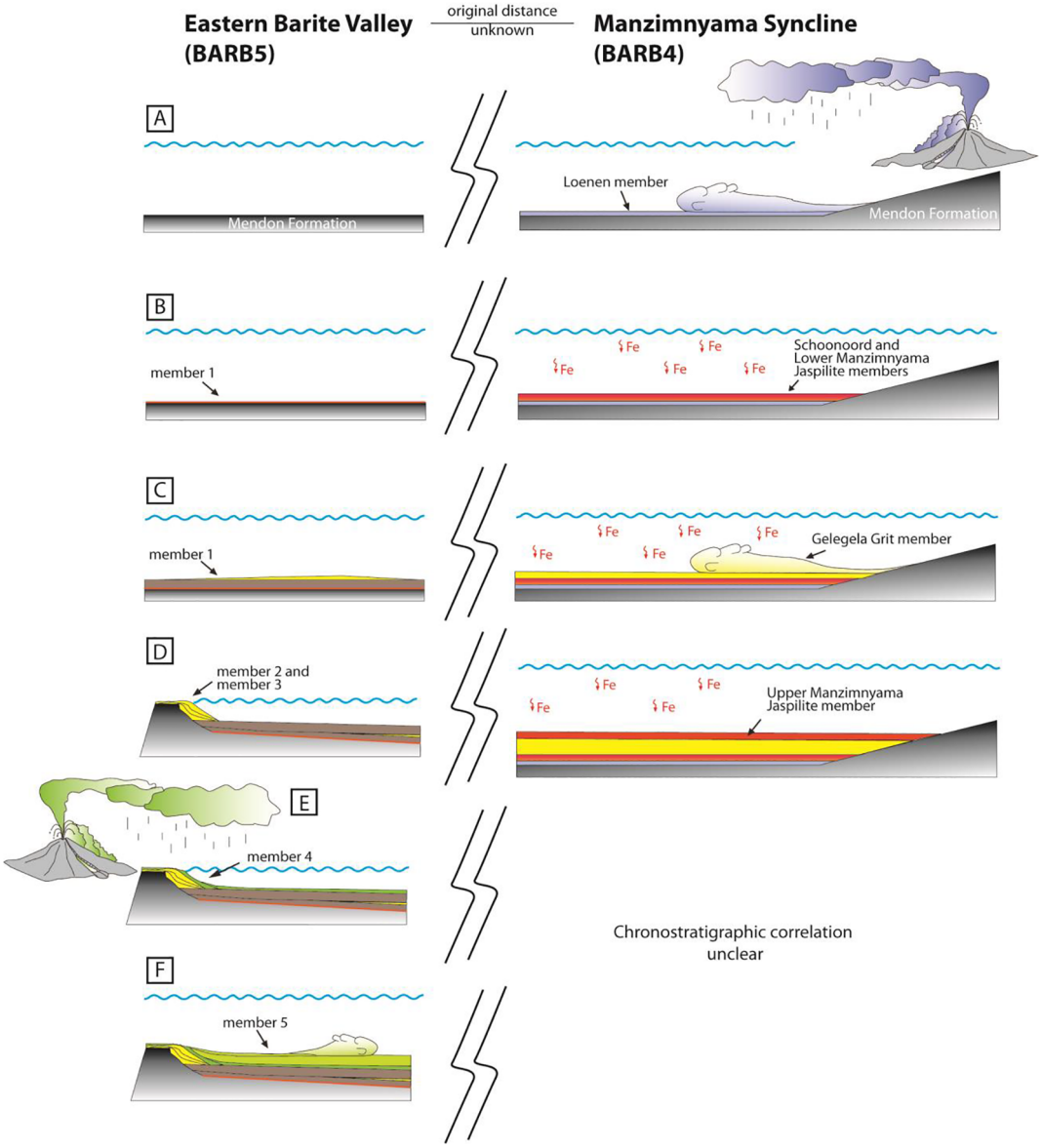

Fig. 13. Schematic illustration of the evolution of the Mapepe Formation in the MS and the EBV. The original distance between the two areas is unknown, making it possible that they initially formed one large basin or two unrelated basins. Similarly, the relative position of the sediment feeder systems is unclear. In the EBV, it may have been located to the northwest or southeast. In the MS, the lack of current structures and indicative facies relationships precludes the positioning of the feeder system. [A] Sedimentation commenced as early as 3277 Ma in the MS with the deposition of the reworked rhyolitic tuff of the Loenen member. No Mapepe sedimentation occurred at that time in the EBV. [B] Deposition of iron-oxyhydroxides commenced in the MS during the deposition of the Schoonoord and the Lower Manzimnyama Jaspilite members and continues throughout Mapepe time. The lower jaspilite yields an age of 3260 ± 5 Ma (Byerly, pers. commun.), suggesting that sedimentation of member 1 in the EBV commenced concurrently. [C] Deep-water sedimentation persisted in both areas during deposition of the Gelegela Grit member in the MS and member 1 in the EBV. These two units may be lithostratigraphically correlative. [D] In the EBV at approx. 3.24 Ga, shallow uplift of upper rocks of the Mendon Formation initiated the formation of a small-scale fan-delta. Meanwhile, deep-water sedimentation may have continued during the deposition of the Upper Manzimnyama Jaspilite member in the MS. However, the lack of age constraints and marker horizons also makes it possible that all MS strata were deposited prior to 3.24 Ga. [E] The EBV area was draped by dacitic volcaniclastic debris at 3239 Ma. No evidence for dacitic volcanism is preserved in the MS, either suggesting that the two areas lay far apart or that the upper part of the MS was not preserved. [F] At 3235 Ma, the platform in the EBV area is drowned by relative sea-level rise during deposition of member 5. Sedimentation in the EBV continues until 3227 Ma (Kröner et al., 1991).

geochemistry, and detrital zircon geochronology, that is very different from that seen in the MS (Figs. 12 and 13). Member 1 at the base of the core (760–460 m core depth) is composed of mudstone and fine-grained sandstone deposited by hemipelagic rain-out and low-density turbidity currents. The sandstone shows a mixed volcanic and sedimentary lithic framework mode and the mudstone geochemistry reveals a mixed mafic and felsic provenance. A detrital zircon sample from the base of member 1, 3 m above the S2 spherule bed that marks the base of the Mapepe Formation, had a low zircon yield (n = 10) with four zircon grains of Fig Tree-age with a mean weighted average age of 3257 ± 6 Ma which coincides with the inferred onset of Mapepe deposition in the EBV area at ~3.26 Ga based on the age of the S2 spherule bed.

The shallow-water siliciclastic sandstone of member 3 in BARB5 (400–261 m core depth) is composed exclusively of carbonaceous and translucent chert grains and contains a major 3288 ± 1 Ma Mendon-age detrital zircon peak, suggesting that chert of the upper Mendon Formation was the dominant source for these sands. The associated mudstone is consistent in indicating a basaltic to komatiitic source component, almost certainly represented by thick sections of komatiitic

volcanic rock in the Mendon Formation. The youngest zircon peak age of 3249 ± 6 Ma (at 376–359 m core depth) is within error of the underlying S3 spherule bed (at 512 m core depth), which has been dated at 3243 ± 4 Ma (Kröner et al., 1991).

Member 4 (261–110 m) marks the abrupt influx of dacitic volcaniclastic debris. Most member 4 sandstone units contain volcanic quartz, recognizable volcanic lithic grains, and replaced plagioclase and represents dacitic tuff and only slightly reworked dacitic ash. The only evidence for non-felsic volcanic debris comes from the presence of Cr-spinels in heavy-mineral lag deposits, trace amounts of gold, molybdenite, magnetite and ilmenite grains (Heinrichs and Reimer, 1977), and potentially by the presence of older zircon clusters. The youngest peak age of the detrital zircon grains in sample BARB5-DZ4 indicates a depositional age of 3239 ± 1 Ma.

Member 5 at the top of the EBV section (> 110 m) is present only in the drill core and not exposed in outcrop. The sandstone is a mixture of dacitic volcanic grains, volcanic quartz, partially to completely replaced plagioclase, carbonaceous chert, and translucent chert grains. Immobile element ratios and REE (Figs. 8–10) indicate a high contribution of dacitic volcanic material and a reduced mafic input relative to mudstone lower in the section. The detrital zircon age spectrum reveals a prominent Fig Tree-age peak at 3235 ± 1 Ma, which we interpret as the maximum depositional age. Additional older peaks of Hooggenoeg and Theespruit age are present in member 5 as well. Based on this provenance signal, the sediments were eroded primarily from the immediately underlying dacitic tuff and penecontemporaneous dacitic volcanic rocks and secondarily from banded cherts of the Onverwacht Group.

Overall, the Mapepe deposits in the EBV are characterized by rapid lateral facies changes and mark a period of mainly local uplifts, erosion of the underlying Mendon Formation, dacitic volcanic activity, and generally short-distance transport of sediment. There is little evidence for large, integrated drainage systems (Drabon, 2018) and the mixing of sediment from broad, regional sources

6.5. Correlation of Manzimnyama and Barite Valley structural belts

Correlation between the studied sections of the Mapepe Formation in the MS and the EBV is problematic due to the lack of chronostratigraphic marker horizons and meaningful depositional ages in the upper part of the MS sequence (Fig. 12). The two sequences show significant differences in the timing of the onset of Mapepe sedimentation, provenance, and depositional environment (Fig. 13). Deposition in the MS commenced at about 3.28 Ga, possibly up to 17 m.yr. before sedimentation in the EBV, which was initiated immediately following the S2 impact at 3.26 Ga. The entire MS section, including the BARB4 drill core section, was deposited under deep-water conditions and was characterized by deposition of iron-rich chemical and detrital sediments, including > 100 m-thick units of BIF, BFC and chamosite-bearing sandstone. In contrast, the EBV sequence lacks the rhyolitic felsic unit seen at the base of the MS sequence; while the lower part of the EBV section was deposited below wave base similar to the MS sequence, it lacks iron-rich strata. The middle and upper parts of the EBV section were deposited in shallow-water and fan-delta settings (Drabon, 2018) and involved the deposition of large volumes of fresh dacitic ash that is absent in the MS.

Only the Lower Manzimnyama Jaspilite and Gelegela Grit members in the MS and member 1 in the EBV display three similar provenance indicators and may thus be correlative: (1) Sandstones in both units represent mixtures of immature sedimentary and volcanic lithic material. (2) The LREE of shales in both units are moderately fractionated, the HREE are flat (Fig. 10), and they show a similar pattern in the La_N/Yb_N vs. Th/Sc plot (Fig. 9), indicating that both represent a mixture of felsic to ultramafic source rocks. (3) Finally, the units in the MS and the turbiditic sandstone in member 1 of the EBV section show the same detrital zircon age distribution (Fig. 11). The two sequences may thus have formed within in a single basin that was coherent for 30 million years, but only the EBV area was affected by local uplifts, shifting depositional centers and volcanic activity during middle and late Mapepe time. However, an unambiguous correlation between these units is not possible for several reasons: Firstly, while both units were deposited in relatively deep water, the EBV lacks the pervasive abundance of iron, including BIF, BFC, iron-rich mudstone, and chamosite grains in turbiditic sandstone observed in the MS. These differences clearly require very different environmental conditions at the time of deposition. Secondly, the 3.45 Ga and 3.55 Ga old zircon grains that occur in sandstones both in the MS and EBV are nearly ubiquitous components of both Fig Tree and Moodies sandstones across the BGB even in unrelated depositional systems (Drabon et al., 2017). They do not necessarily carry correlation-relevant information.

A correlation between the upper part of the MS is particularly problematic due to the paucity of datable rocks and the absence of chronostratigraphic marker horizons. It is possible that the entire MS sedimentary sequence is time-correlative with only the lower mudstone member 1 of the EBV sequence with the upper part of the MS not being preserved. This scenario would provide an explanation for the apparent absence of the S3 spherule bed and the lack of penecontemporaneous Fig Tree dacitic volcaniclastic rocks in the MS section because all of these EBV units are stratigraphically younger than any dated units in the MS. However uncertain the correlation between these sections, it is clear that the two sequences are not entirely chronostratigraphically correlative as previously assumed (Heinrichs and Reimer, 1977; Lowe and Nocita, 1999).

We are struck by the contrast between the Mapepe sections in the EBV and MS in terms of onset of sedimentation, depositional environments, abundance of iron, and presence of much younger Fig Tree volcaniclastic rocks in the EBV. These contrasts suggest that either these structural belts were originally far apart and were juxtaposed during post-depositional shortening in late- and post-Fig Tree time (e.g., Ramsay, 1963; Heubeck and Lowe, 1994; Lowe et al., 1999) or that they represent very contrasting and separate parts of a single large, complex basin.

6.6. Nature of uplift during the Mapepe time

The onset of the Mapepe deposition marks an abrupt sedimentological, volcanic, and tectonic transition in the evolution of the BGB. During Onverwacht time, sedimentation during accumulation of mafic and ultramafic flow sequences was dominated by three main sediment types: chemical sedimentation, deposition of mainly fine-grained pyroclastic and volcaniclastic debris, and biogenic sedimentation (Lowe, 1999). Relief was limited mainly to the build-up of felsic volcanic complexes, which sourced coarse felsic debris to surrounding sedimentary aprons. Siliciclastic sediments derived by uplift, weathering, and erosion are rare. After 300 million years of this style of sedimentation, the transition to Fig Tree sedimentation was marked by the sudden appearance of tectonic surface relief that sourced an influx of terrigenous sediments. At this same time, basaltic and komatiitic volcanism ceased regionally and probably permanently.

The results of this study reveal several insights into the nature of the onset of crustal uplift. Mapepe sediments were mainly sourced locally, as suggested by the presence of relatively thin lenticular packages of immature sandstone and conglomerate that differ in sand and conglomerate composition on a small scale, both laterally and vertically, and by the textural and compositional immaturity of the sandstone. This argues for many local and shallow uplifts that exposed rocks of the underlying parts of the upper Onverwacht Group, especially underlying Mendon strata, and hosted small sediment drainage systems. Changes in provenance in the EBV and MS sediments are characterized by sharp contacts suggesting that sudden changes occurred in the source terrane and indicating that uplift was rather local and abrupt. Besides the local influx of debris from the upper Onverwacht Group, a common

characteristic of the MS, EBV, and other structural belts throughout the BGB (Drabon et al., 2017) is the ubiquitous presence of detrital zircon grains of upper Hooggenoeg and Theespruit Formation ages. This may suggest that uplifted rocks of the lower Onverwacht Group were permanently exposed in the hinterland and distributed sediments regionally to the Mapepe sedimentary system. Alternatively, these zircon grains may represent xenocrysts that were incorporated into younger magmas during their ascent through older magmatic units in the root of the BGB (Byerly et al., 1996) and thus do not carry any information regarding their provenance.

Several tectonic models for the Fig Tree Group have been proposed. These range from geodynamic settings associated with either a continental crust (e.g., Condie and Hunter, 1976; Eriksson, 1980; Kröner et al., 2013, 2016) or juvenile crust (e.g., De Wit et al., 1987; Lowe and Nocita, 1999; Moyen et al., 2006; Schoene et al., 2008; Schoene and Bowring, 2010; Sanchez-Garrido et al., 2011) and different modern-style plate tectonic processes ranging from compressional (e.g., De Wit et al., 1987; Lowe and Nocita, 1999; Moyen et al., 2006; Schoene et al., 2008; Schoene and Bowring, 2010) to extensional (e.g., Condie and Hunter, 1976; Eriksson, 1980). Additionally, several authors have suggested that the Fig Tree basins formed by gravitational overturn in the absence of modern-style plate tectonics (e.g., Anhaeusser, 2010; Van Kranendonk, 2011). Although the tectonic setting of the Fig Tree Group cannot be constrained by the data presented here, a comparison of studies of the Mapepe Formation (Nocita and Lowe, 1990; Lowe and Nocita, 1999; Lowe, 2013) shows that the onset of tectonic deformation was regionally characterized by the formation of numerous small-scale local uplifts. Exposures of sources to Mapepe sediments have been documented in only one area, where the S2 impact triggered fracturing of the upper rigid crust and the formation of local relief that sourced adjacent fan-delta sediments in the lower Mapepe Formation (Lowe, 2013; Sleep and Lowe, 2014). Throughout most of the BGB, the onset of Fig Tree orogenesis (D2 of De Ronde and Wit, 1994, Lowe et al., 1999, Byerly et al., 2018) is marked by the deposition of spherules. The clustering of meteorite impacts, including the S2, S3, and possibly S4 impacts between 3.26 and 3.24 Ga, the cessation of mafic and ultramafic volcanism, and initiation of regional uplift suggest a causal relationship. They offer the prospect that large impacts may have directly or indirectly triggered crustal deformation and uplift associated with Fig Tree deposition (Glikson, 2001, 2008; Glikson and Vickers, 2006; Lowe et al., 2003; Lowe, 2013) and that early Fig Tree uplift may rather reflect impact events than internal tectonic processes.

7. Summary and conclusions

Siliciclastic sedimentary rocks of the Mapepe Formation were sourced by uplifts of supracrustal sedimentary and volcanic rocks of the Barberton Supergroup. They represent immature first-cycle sediments that did not undergo prolonged transport or recycling. During uplift and erosion represented by detrital sedimentary rocks of the Mapepe Formation, erosion had not reached deeper-seated plutonic rocks and there is no evidence that the AGC or comparable high-grade, coarse-grained metamorphic rocks provided sediments to the Mapepe basin. There is no evidence that the sedimentary rocks of the Mapepe Formation were derived from a continental terrane.

Comparison of the BARB4 and BARB5 cores reveals significant differences between the EBV and the MS structural belts: (1) Deposition of the sediments in the MS commenced up to about 17 Ma prior to deposition in the EBV. (2) BARB4 shows an evolution from rhyolitic sources upward to a dominantly mafic provenance. In contrast, EBV sedimentary rocks display a transition from a dominantly more basaltic and komatiitic provenance to a dacitic provenance. (3) Strata in the MS section were deposited in a deep-water setting throughout their accumulation whereas EBV rocks reflect an initial deep-water setting but rapidly evolved into predominantly shallow-water and intertidal units. (4) Sandstone throughout the MS displays a mixed provenance of silicified rocks of the Onverwacht Group, while individual sandstone units in the EBV are distinct in composition and were dominantly supplied by local erosion of immediately underlying sedimentary or volcanic rocks. (5) The Mapepe section in the EBV lacks the thick accumulation of iron-rich chemical sediments, including BFC, BIF, and chamosite that are abundant in the MS section. Only the middle parts of the MS sequence (the Lower Manzimnyama Jaspilite and the Gelegela Grit members) and the basal sedimentary rocks in the EBV (member 1) show similar petrography, geochemistry, and depositional age, and may have been related. However, the lithologies of these two units vary significantly, suggesting that they were not deposited in spatial proximity but instead formed significantly apart, were separated by a paleogeographic barrier, or formed as unrelated sequences that have since been juxtaposed by faulting. A chrono- and lithostratigraphic correlation between the Mapepe rocks higher in the section is problematic due to the paucity of datable rocks in the MS and the absence of chronostratigraphic marker horizons.

Overall, the provenance of Mapepe sediments throughout the BGB argues for the presence of numerous local, small uplifts and deposition in adjacent fan-deltas that pass laterally into deeper-water environments. The results of this study suggest that the Mapepe Formation may not have been deposited as a single connected sedimentary system and that previous basin reconstructions, which assume synchronicity of Mapepe deposition among the various BGB structural belts, need to be carefully reevaluated.

Acknowledgements

We thank the ICDP (International Continental Scientific Drilling Program) for providing funds for drilling the Barberton BARB4 and BARB5 wells and sappi and the Mpumalanga Tourism and Parks Agency for access to lands. Funding for travel expenses and analytical costs were kindly provided by the School of Earth, Energy, and Environmental Sciences and the Center for African Studies at Stanford University. We also thank Hervé Wabo for help during sampling the BARB4 and BARB5 cores and Trevor Dumitru for help during mineral separation. The staff of the Arizona LaserChron Center at the University of Arizona and Matthew Coble at the SHRIMP-RG laboratory at Stanford University were very helpful during detrital zircon analyses. Fieldwork for P.M. and A.G. was supported by the Dr. Schürmann Foundation. This paper benefited from discussions with Gary R. Byerly and Marty Grove. We thank Christoph Heubeck and an anonymous reviewer for their comments that substantially improved the manuscript.

Appendix A. Supplementary material

Supplementary data to this article can be found online at https://doi.org/10.1016/j.precamres.2019.02.010.

References

Anhaeusser, C.R., Robb, L.J., Viljoen, M.J., 1983. Notes on the provisional geological map of the Barberton greenstone belt and surrounding granitic terrane, eastern Transvaal and Swaziland (1:250,000 colour map). Spec. Publ. Geol. Soc. South Africa 9, 221–223.

Anhaeusser, C.R., 2010. Magmatic and structural characteristics of the ca. 3440 Ma Theespruit pluton, Barberton Mountain Land, South Africa. Am. J. Sci. 310 (9), 1136–1167.

Armstrong, R.A., Compston, W., De Wit, M.J., Williams, I.S., 1990. The stratigraphy of the 3.5-3.2 Ga Barberton Greenstone Belt revisited: a single zircon ion microprobe study. Earth Planet. Sci. Lett. 101 (1), 90–106.

Berry, R.F., Jenner, G.A., Meffre, S., Tubrett, M.N., 2001. A North American provenance for Neoproterozoic to Cambrian sandstones in Tasmania? Earth Planet Sci. Lett. 192, 207–222.

Bouma, A.H., 1962. Sedimentology of Some Flysch Deposits; A Graphic Approach to Facies Interpretation. Published PhD dissertation. Elsevier, pp. 168.

Byerly, G.R., Kröner, A., Lowe, D.R., Todt, W., Walsh, M.M., 1996. Prolonged magmatism and time constraints for sediment deposition in the early Archean Barberton greenstone belt: evidence from the Upper Onverwacht and Fig Tree groups. Precambr. Res.

78 (1–3), 125–138.
Byerly, G.R., Lowe, D.R., Heubeck, C.E., 2018. Geologic evolution of the Barberton greenstone BeltdA unique record of crustal development, surface processes, and early life 3.55e3.20 Ga. In: Van Kranendonk, M.J., Bennett, V., Hoffmann, E. (Eds.), Earth's Oldest Rocks, pp. 569–613.
Condie, K.C., Macke, J.E., Reimer, T.O., 1970. Petrology and geochemistry of early Precambrian graywackes from the Fig Tree Group, South Africa. Geol. Soc. Am. Bull. 81, 2759–2776.
Crowley, J.L., Schoene, B., Bowring, S.A., 2007. U-Pb dating of zircon in the Bishop Tuff at the millennial scale. Geology 35 (12), 1123–1126.
Condie, K.C., Hunter, D.R., 1976. Trace element geochemistry of Archean granitic rocks from the Barberton region, South Africa. Earth Planet. Sci. Lett. 29 (2), 389–400.
Dai, S., Chou, C.L., 2007. Occurrence and origin of minerals in a chamosite-bearing coal of Late Permian age, Zhaotong, Yunnan, China. Am. Mineral. 92 (8–9), 1253–1261.
De Ronde, C.E.J., Hall, C.M., York, D., Spooner, E.T.C., 1991. LASER step-heating 40Ar/39Ar age spectra from early Archean (~ 3.5 Ga) Barberton greenstone belt sediments: a technique for detecting cryptic tectono-thermal events. Geochim. Cosmochim. Acta 55 (7), 1933–1951.
De Ronde, C.E., Wit, M.J., 1994. Tectonic history of the Barberton greenstone belt, South Africa: 490 million years of Archean crustal evolution. Tectonics 13 (4), 983–1005.
Decker, N.B., Byerly, G.R., Stiegler, M.T., Lowe, D.R., Stefurak, E., 2015. High resolution tephra and U/Pb chronology of the 3.33–3.26 Ga Mendon Formation, Barberton Greenstone Belt, South Africa. Precambr. Res. 261, 54–74.
De Wit, M.J., Hart, R.A., Hart, R.J., 1987. The Jamestown Ophiolite Complex, Barberton mountain belt: a section through 35 Ga oceanic crust. J. Afr. Earth Sci. (1983) 6 (5), 681–730.
Dickinson, W.R., 1970. Interpreting detrital modes of graywacke and arkose. J. Sediment. Res. 40 (2), 695–707.
Dickinson, W.R., Suczek, C.A., 1979. Plate tectonics and sandstone compositions. AAPG Bull. 63 (12), 2164–2182.
Dickinson, W.R., 1985. Interpreting provenance relations from detrital modes of sandstones. In: Zuffa, G.G. (Ed.), Provenance of Arenites. Reidel Publications, Springer, Dordrecht, pp. 333–361.
Drabon, N., Lowe, D.R., Byerly, G.R., Harrington, J.A., 2017. Detrital zircon geochronology of sandstones of the 3.6–3.2 Ga Barberton greenstone belt: no evidence for older continental crust. Geology 45 (9), 803–806.
Drabon, N., 2018. Crustal Setting, Provenance, and Sedimentation in the Paleoarchean Barberton Greenstone Belt, South Africa. PhD Thesis. Stanford University, pp. 360.
Duchac, K.C., 1986. Metasomatic Alteration of a Komatiitic Sequence into Chert, Barberton Mountain Land, South Africa. Doctoral dissertation. Louisiana State University, Baton Rouge.
Duchac, K.C., Hanor, J.S., 1987. Origin and timing of the metasomatic silicification of an early Archean komatiite sequence, Barberton Mountain Land, South Africa. Precambr. Res. 37 (2), 125–146.
Eriksson, K.A., 1980. Transitional sedimentation styles in the Moodies and Fig Tree Groups, Barberton Mountain Land, South Africa: evidence favouring an Archean continental margin. Precambr. Res. 12 (1), 141–160.
Farber, K., Dziggel, A., Meyer, F.M., Harris, C., 2016. Petrology, geochemistry and fluid inclusion analysis of altered komatiites of the Mendon Formation in the BARB4 drill core, Barberton greenstone belt, South Africa. S. Afr. J. Geol. 119 (4), 639–654.
Fritz, J., Tagle, R., Ashworth, L., Schmitt, R.T., Hofmann, A., Luais, B., Harris, P.D., Hoehnel, D., Özdemir, S., Mohr-Westheide, T., Koeberl, C., 2016. Nondestructive spectroscopic and petrochemical investigations of Paleoarchean spherule layers from the ICDP drill core BARB5, Barberton Mountain Land, South Africa. Meteorit. Planet. Sci. 51 (12), 2441–2458.
Galić, A., 2015. Unravelling Atmospheric Photolysis and Ocean Redox Chemistry from Paleoarchean Pyrite: A Multiple Sulfur and Iron Stable Isotope Study. PhD thesis. Utrecht University, The Netherlands, pp. 175.
Gehrels, G.E., Valencia, V.A., Ruiz, J., 2008. Enhanced precision, accuracy, efficiency, and spatial resolution of U-Pb ages by laser ablation–multicollector–inductively coupled plasma–mass spectrometry. Geochem. Geophys. Geosyst. 9 (3), 1–13.
Gehrels, G., Pecha, M., 2014. Detrital zircon U-Pb geochronology and Hf isotope geochemistry of Paleozoic and Triassic passive margin strata of western North America. Geosphere 10 (1), 49–65.
Grosch, E.G., Kosler, J., McLoughlin, N., Drost, K., Slama, J., Pedersen, R.B., 2011. Paleoarchean detrital zircon ages from the earliest tectonic basin in the Barberton Greenstone Belt, Kaapvaal craton, South Africa. Precambr. Res. 191 (1–2), 85–99.
Glikson, A.Y., 2001. The astronomical connection of terrestrial evolution: crustal effects of post-3.8 Ga mega-impact clusters and evidence for major 3.2 ± 0.1 Ga bombardment of the Earth-Moon system. J. Geodyn. 32, 205–229.
Glikson, A.Y., 2008. Field evidence of Eros-scale asteroids and impact-forcing of Precambrian geodynamic episodes, Kaapvaal (South Africa) and Pilbara (Western Australia) Cratons. Earth Planet. Sci. Lett. 267, 558–570.
Glikson, A., Vickers, J., 2006. The 3.26–3.24 Ga Barberton asteroid impact cluster: tests of tectonic and magmatic consequences, Pilbara Craton, Western Australia. Earth Planet. Sci. Lett. 241, 11–20.
Harrington, J.A., 2017. Using sedimentology and provenance studies to determine depositional relationships between three structural belts of the ca. 3.22 Ga Fig Tree Group, Barberton Greenstone Belt, South Africa. MSc Thesis. Stanford University, pp. 93.
Heubeck, C., 2019. The Moodies Group - A high-resolution archive of Archaean surface and basin-forming processes. In: Kröner, A., Hofmann, A. (Eds.), The Archaean Geology of the Kaapvaal Craton, Southern Africa. Springer (Regional Geology Reviews), pp. 203–241.
Heubeck, C., Lowe, D.R., 1994. Late syndepositional deformation and detachment tectonics in the Barberton Greenstone Belt, South Africa. Tectonics 13 (6), 1514–1536.
Heubeck, C., Lowe, D.R., 1999. Sedimentary petrography and provenance of the Archean Moodies Group, Barberton Greenstone Belt. Special Paper – Geol. Soc. Am. 329, 259–286.
Heinrichs, T., 1980. Lithostratigraphische Untersuchungen in der Fig Tree Gruppe des Barberton Greenstone Belt zwischen Umsoli und Lomati (Südafrika). Selbstverlag des Geologisch-Paläontologischen Instituts der Georg-August-Universität Göttingen 22, 128.
Heinrichs, T.K., Reimer, T., 1977. A sedimentary barite deposit from the Archean Fig Tree Group of the Barberton Mountain Land (South Africa). Econ. Geol. 72 (8), 1426–1441.
Hessler, A.M., Lowe, D.R., 2006. Weathering and sediment generation in the Archean: an integrated study of the evolution of siliciclastic sedimentary rocks of the 3.2 Ga Moodies Group, Barberton Greenstone Belt, South Africa. Precambr. Res. 151 (3–4), 185–210.
Hofmann, A., 2005. The geochemistry of sedimentary rocks from the Fig Tree Group, Barberton greenstone belt: implications for tectonic, hydrothermal and surface processes during mid-Archaean times. Precambr. Res. 143 (1), 23–49.
Hofmann, A., Harris, C., 2008. Silica alteration zones in the Barberton greenstone belt: a window into subseafloor processes 3.5–3.3 Ga ago. Chem. Geol. 257 (3), 221–239.
Hunter, D.R., Barker, F., Millard Jr, H.T., 1978. The geochemical nature of the Archean Ancient Gneiss Complex and Granodiorite Suite, Swaziland: a preliminary study. Precambr. Res. 7 (2), 105–127.
Ingersoll, R.V., Fullard, T.F., Ford, R.L., Grimm, J.P., Pickle, J.D., Sares, S.W., 1984. The effect of grain size on detrital modes; a test of the Gazzi-Dickinson point-counting method. J. Sediment. Res. 54 (1), 103–116.
Jackson, M.P.A., Eriksson, K.A., Harris, C.W., 1987. Early Archean foredeep sedimentation related to crustal shortening: a reinterpretation of the Barberton Sequence, southern Africa. Tectonophysics 136 (3–4), 197–221.
Kisters, A.F., Stevens, G., Dziggel, A., Armstrong, R.A., 2003. Extensional detachment faulting and core-complex formation in the southern Barberton granite–greenstone terrain, South Africa: evidence for a 3.2 Ga orogenic collapse. Precambr. Res. 127 (4), 355–378.
Kleinhanns, I.C., Kramers, J.D., Kamber, B.S., 2003. Importance of water for Archaean granitoid petrology: a comparative study of TTG and potassic granitoids from Barberton Mountain Land, South Africa. Contrib. Miner. Petrol. 145 (3), 377–389.
Knauth, L.P., Lowe, D.R., 1978. Oxygen isotope geochemistry of cherts from the Onverwacht Group (3.4 billion years), Transvaal, South Africa, with implications for secular variations in the isotopic composition of cherts. Earth Planet. Sci. Lett. 41 (2), 209–222.
Kohler, E.A., Anhaeusser, C.R., 2002. Geology and geodynamic setting of Archaean silicic metavolcaniclastic rocks of the Bien Venue Formation, Fig Tree Group, northeast Barberton greenstone belt, South Africa. Precambr. Res. 116 (3–4), 199–235.
Koeberl, C., Schulz, T., Reimold, W.U., 2015. Remnants of Early Archean impact deposits on Earth: Search for a meteoritic component in the BARB5 and CT3 drill cores (Barberton Greenstone Belt, South Africa). Proc. Eng. 103, 310–317.
Konhauser, K.O., Lalonde, S.V., Planavsky, N.J., Pecoits, E., Lyons, T.W., Mojzsis, S.J., Rouxel, O.J., Barley, M.E., Rosière, C., Fralick, P.W., Kump, L.R., 2011. Aerobic bacterial pyrite oxidation and acid rock drainage during the Great Oxidation Event. Nature 478 (7369), 369.
Kröner, A., Anhaeusser, C.R., Hoffmann, J.E., Wong, J., Geng, H., Hegner, E., Xie, H., Yang, J., Liu, D., 2016. Chronology of the oldest supracrustal sequences in the Palaeoarchaean Barberton Greenstone Belt, South Africa and Swaziland. Precambr. Res. 279, 123–143.
Kröner, A., Byerly, G.R., Lowe, D.R., 1991. Chronology of early Archaean granite-greenstone evolution in the Barberton Mountain Land, South Africa, based on precise dating by single zircon evaporation. Earth Planet. Sci. Lett. 103 (1–4), 41–54.
Kröner, A., Hegner, E., Wendt, J.I., Byerly, G.R., 1996. The oldest part of the Barberton granitoid-greenstone terrain, South Africa: evidence for crust formation between 3.5 and 3.7 Ga. Precambr. Res. 78 (1–3), 105–124.
Kröner, A., Hoffmann, J.E., Xie, H., Wu, F., Münker, C., Hegner, E., Wong, J., Wan, Y., Liu, D., 2013. Generation of early Archaean felsic greenstone volcanic rocks through crustal melting in the Kaapvaal Craton, southern Africa. Earth and Planetary Science Letters 381, 188–197.
Kröner, A., Todt, W., 1988. Single zircon dating constraining the maximum age of the Barberton greenstone belt, southern Africa. J. Geophys. Res. Solid Earth 93 (B12), 15329–15337.
Lahaye, Y., Arndt, N., Byerly, G., Chauvel, C., Fourcade, S., Gruau, G., 1995. The influence of alteration on the trace-element and Nd isotopic compositions of komatiites. Chem. Geol. 126 (1), 43–64.
Lowe, D.R., 1999. Geologic evolution of the Barberton Greenstone Belt and vicinity. Special Paper – Geol. Soc. Am. 329, 287–312.
Lowe, D.R., 2013. Crustal fracturing and chert dike formation triggered by large meteorite impacts, ca. 3.260 Ga, Barberton greenstone belt, South Africa. Geol. Soc. Am. Bull. 125, 894–912.
Lowe, D.R., Byerly, G.R., 1986. Archaean flow-top alteration zones formed initially in a low-temperature sulphate-rich environment. Nature 324 (6094), 245–248.
Lowe, D.R., Byerly, G.R., 1999. Stratigraphy of the west-central part of the Barberton Greenstone Belt, South Africa. Special Paper – Geol. Soc. Am. 329, 1–36.
Lowe, D.R., Byerly, G.R., Heubeck, C., 1999. Structural divisions and development of the west-central part of the Barberton Greenstone Belt. Special Paper – Geol. Soc. Am. 329, 37–82.
Lowe, D.R., Byerly, G.R., Heubeck, C., 2012. Geologic map of the Barberton Greenstone Belt, Map and chart series MCH103. Geological Society of America.
Lowe, D.R., Byerly, G.R., Kyte, F.T., Shukolyukov, A., Asaro, F., Krull, A., 2003. Spherule beds 3.47–3.24 billion years old in the Barberton Greenstone Belt, South Africa: a record of large meteorite impacts and their influence on early crustal and biological

evolution. Astrobiology 3 (1), 7–48.
Lowe, D.R., Nocita, B.W., 1999. Foreland basin sedimentation in the Mapepe Formation, southern-facies Fig Tree Group. Special Paper – Geol. Soc. Am. 329, 233–258.
Ludwig, K.R., 2001. SQUID 1.02 A user's manual. Geochronological Center, Berkeley.
Ludwig, K.R., 2003. User's manual for IsoPlot 3.0. A Geochronological Toolkit for Microsoft Excel, 71.
MacGeehan, P.J., MacLean, W.H., 1980. An Archaean sub-seafloor geothermal system, 'calc-alkali'trends, and massive sulphide genesis. Nature 286 (5775), 767.
Mohr-Westheide, T., Reimold, W.U., Fritz, J., Koeberl, C., Salge, T., Hofmann, A., Schmitt, R.T., 2015. Discovery of extraterrestrial component carrier phases in Archean spherule layers: implications for estimation of Archean bolide sizes. Geology 43 (4), 299–302.
Moyen, J.F., Stevens, G., Kisters, A., 2006. Record of mid-Archaean subduction from metamorphism in the Barberton terrain, South Africa. Nature 442 (7102), 559.
Mücke, A., 2006. Chamosite, siderite and the environmental conditions of their formation in chamosite-type Phanerozoic ooidal ironstones. Ore Geol. Rev. 28 (2), 235–249.
Nesbitt, H., Young, G.M., 1982. Early Proterozoic climates and plate motions inferred from major element chemistry of lutites. Nature 299 (5885), 715–717.
Nocita, B.W., 1989. Sandstone petrology of the Archean Fig Tree Group, Barberton greenstone belt, South Africa: tectonic implications. Geology 17, 953–956.
Nocita, B.W., Lowe, D.R., 1990. Fan-delta sequence in the Archean Fig Tree Group, Barberton greenstone belt, South Africa. Precambr. Res. 48 (4), 375–393.
Nutman, A.P., 2001. On the scarcity of > 3900 Ma detrital zircons in ≥3500 Ma metasediments. Precambr. Res. 105 (2–4), 93–114.
Pearce, J.A., Cann, J.R., 1973. Tectonic setting of basic volcanic rocks determined using trace element analyses. Earth Planet. Sci. Lett. 19 (2), 290–300.
Premo, W.R., Castiñeiras, P., Wooden, J.L., 2008. SHRIMP-RG U-Pb isotopic systematics of zircon from the Angel Lake orthogneiss, East Humboldt Range, Nevada: is this really Archean crust. Geosphere 4 (6), 963–975.
Press, W.H., Teukolosky, S.A., Vetterling, W.T., Flannery, B.P., 1997. Numerical Recipes in C: The Art of Scientific Computing. Cambridge University Press, Cambridge, pp. 994.
Ramsay, J.G., 1963. Structural Investigations in the Barberton Mountain Land, Eastern Transvaal. S. Afr. J. Geol. 66 (Transactions 1963), 353–401.
Reimer, T.O., 1967. Die Geologie der Stolzburg Synklinale im Barberton Bergland (Transvaal-Südafrika), Diplom-Arbeit (unpublished), Goethe-Universität Frankfurt, p. 103.
Reimer, T.O., 1972. Diagenetic reactions in early Precambrian graywackes of the Barberton Mountain land (South Africa). Sed. Geol. 7 (4), 263–282.
Reimer, T.O., 1975. Untersuchungen über Abtragung, Sedimentation und Diagenese im frühen Präkambrium am Beispiel der Sheba-Formation (Südafrika). Geologisches Jahrbuch, Reihe B 17, 108.
Reimer, T.O., 1980. Archean sedimentary baryte deposits of the Swaziland Supergroup (Barberton Mountain Land, South Africa). Precambr. Res. 12, 393–410.
Reimer, T.O., 1983. Pseudo-oolites in rocks of the Ulundi Formation, lower part of the Archaean Fig Tree Group (South Africa). Precambr. Res. 20, 375–390.
Rivas-Sanchez, M.L., Alva-Valdivia, L.M., Arenas-Alatorre, J., Urrutia-Fucugauchi, J., Ruiz-Sandoval, M., Ramos-Molina, M.A., 2006. Berthierine and chamosite hydrothermal: genetic guides in the Peña Colorada magnetite-bearing ore deposit, Mexico. Earth Planets Space 58 (10), 1389–1400.
Roerdink, D.L., Mason, P.R., Whitehouse, M.J., Brouwer, F.M., 2016. Reworking of atmospheric sulfur in a Paleoarchean hydrothermal system at Londozi, Barberton Greenstone Belt, Swaziland. Precambr. Res. 280, 195–204.
Sanchez-Garrido, C.J., Stevens, G., Armstrong, R.A., Moyen, J.F., Martin, H., Doucelance, R., 2011. Diversity in Earth's early felsic crust: Paleoarchean peraluminous granites of the Barberton Greenstone Belt. Geology 39 (10), 963–966.
Schoene, B., de Wit, M.J., Bowring, S.A., 2008. Mesoarchean assembly and stabilization of the eastern Kaapvaal craton: a structural-thermochronological perspective. Tectonics 27 (5), 1–27.
Schoene, B., Bowring, S.A., 2010. Rates and mechanisms of Mesoarchean magmatic arc construction, eastern Kaapvaal craton, Swaziland. GSA Bull. 122 (3–4), 408–429.
Schulz, T., Koeberl, C., Luguet, A., van Acken, D., Mohr-Westheide, T., Ozdemir, S., Reimold, W.U., 2017. New constraints on the Paleoarchean meteorite bombardment of the Earth – Geochemistry and Re-Os isotope signatures of spherule layers in the BARB5 ICDP drill core from the Barberton Greenstone Belt, South Africa. Geochim. Cosmochim. Acta 211, 322–340.
Sleep, N.H., Lowe, D.R., 2014. Physics of crustal fracturing and chert dike formation triggered by asteroid impact, ~ 3.26 Ga, Barberton greenstone belt, South Africa. Geochem. Geophys. Geosyst. 15, 1054–1070.
Stevenson, R.K., Patchett, P.J., 1990. Implications for the evolution of continental crust from Hf isotope systematics of Archean detrital zircons. Geochim. Cosmochim. Acta 54 (6), 1683–1697.
Sturesson, U., Heikoop, J.M., Risk, M.J., 2000. Modern and Palaeozoic iron ooids—a similar volcanic origin. Sed. Geol. 136 (1–2), 137–146.
Taylor, J., Zeh, A., Gerdes, A., 2016. U-Pb–Hf isotope systematics of detrital zircons in high-grade paragneisses of the Ancient Gneiss Complex, Swaziland: Evidence for two periods of juvenile crust formation, Paleo- and Mesoarchaean sediment deposition, and 3.23 Ga terrane accretion. Precambr. Res. 280, 205–220.
Taylor, S.R., McLennan, S.M., 1985. The continental Crust: Its Evolution and Composition. Blackwell Scientific, pp. 312.
Taylor, S.R., McLennan, S.M., 1995. The geochemical evolution of the continental crust. Rev. Geophys. 33 (2), 241–265.
Tice, M.M., Bostick, B.C., Lowe, D.R., 2004. Thermal history of the 3.5–3.2 Ga Onverwacht and Fig Tree Groups, Barberton greenstone belt, South Africa, inferred by Raman microspectroscopy of carbonaceous material. Geology 32 (1), 37–40.
Toulkeridis, T., Goldstein, S.L., Clauer, N., Kröner, A., Todt, W., Schidlowski, M., 1998. Sm–Nd, Rb–Sr and Pb–Pb dating of silicic carbonates from the early Archaean Barberton Greenstone Belt, South Africa: evidence for post-depositional isotopic resetting at low temperature. Precambr. Res. 92 (2), 129–144.
Van Schijndel, V., Stevens, G., Zeh, A., Frei, D., Lana, C., 2017. Zircon geochronology and Hf isotopes of the Dwalile Supracrustal Suite, Ancient Gneiss Complex, Swaziland: insights into the diversity of Palaeoarchaean source rocks, depositional and metamorphic ages. Precambr. Res. 295, 48–66.
Van Kranendonk, M.J., 2011. Cool greenstone drips and the role of partial convective overturn in Barberton greenstone belt evolution. J. Afr. Earth Sc. 60 (5), 346–352.
Vennemann, T.W., Smith, H.S., 1999. Geochemistry of mafic and ultramafic rocks in the type section of the Kromberg Formation, Barberton greenstone belt, South Africa. Geol. Soc. Am. Spec. Pap. 329, 133–149.
Xie, X., Byerly, G.R., Ferrell Jr, R.E., 1997. IIb trioctahedral chlorite from the Barberton greenstone belt: crystal structure and rock composition constraints with implications to geothermometry. Contrib. Miner. Petrol. 126 (3), 275–291.
Zentner, D.B., 2014. Stratigraphy, sedimentology and provenance of the ca. 3.26 Ga Mapepe Formation in the Manzimnyama Syncline, Barberton greenstone belt, South Africa. MSc Thesis. Stanford University, pp. 199.